

Candidates for Transiting Planets in OGLE-IV Galactic Bulge Fields

M.J. Mróz¹, P. Pietrukowicz¹, R. Poleski¹, A. Udalski¹,
 M.K. Szymański¹, M. Gromadzki¹, K. Ulaczyk², S. Kozłowski¹,
 J. Skowron¹, D.M. Skowron¹, I. Soszyński¹, P. Mróz¹,
 M. Ratajczak¹, K.A. Rybicki^{1,3}, P. Iwanek¹, M. Wrona¹

¹ Astronomical Observatory, University of Warsaw, Al. Ujazdowskie 4, 00-478
Warszawa, Poland

² Department of Physics, University of Warwick, Coventry CV4 7AL, UK

³ Department of Particle Physics and Astrophysics, Weizmann Institute of Science,
Rehovot 76100, Israel

Received October 9, 2023

ABSTRACT

We present results of a search for transiting exoplanets in 10-yr long photometry with thousands of epochs taken in the direction of the Galactic bulge. This photometry was collected in the fourth phase of the Optical Gravitational Lensing Experiment (OGLE-IV). Our search covered ≈ 222000 stars brighter than $I = 15.5$ mag. Selected transits were verified using a probabilistic method. The search resulted in 99 high-probability candidates for transiting exoplanets. The estimated distances to these targets are between 0.4 kpc and 5.5 kpc, which is a significantly wider range than for previous transit searches. The planets found are Jupiter-size, with the exception of one (named OGLE-TR-1003b) located in the hot Neptune desert. If the candidate is confirmed, it can be important for studies of highly irradiated intermediate-size planets. The existing long-term, high-cadence photometry of our candidates increases the chances of detecting transit timing variations at long timescales. Selected candidates will be observed by the future NASA flagship mission, the Nancy Grace Roman Space Telescope, in its search for Galactic bulge microlensing events, which will further enhance the photometric coverage of these stars.

Key words: *planetary systems – Planets and satellites: detection – Planets and satellites: fundamental parameters – Techniques: photometric*

1. Introduction

Exoplanetary research is one of the most dynamically developing branches of astronomy. At the end of the twentieth century, advances in observing techniques enabled the detection of the first extrasolar planets. Currently, the multitude of exoplanetary discoveries is unprecedented, with the number of confirmed exoplanets

exceeding 5500*. This large number of objects has allowed us to gain a broader understanding of the processes that govern planetary systems, their evolution, and their characteristics. Many studies have shown that planetary systems are much more diverse than our own Solar System (see Zhu and Dong 2021 for a review).

Among the many methods for detecting exoplanets, the transit method plays a crucial role. It is based on observations of regular dimming of a star's brightness due to the presence of a planet blocking part of its light. The method was first used in 1999 to detect a previously known planet around the star HD 209458 (Henry *et al.* 2000, Charbonneau *et al.* 2000). The Optical Gravitational Lensing Experiment (OGLE) was the first survey to successfully apply the transit technique in discovering exoplanets. In observations of millions of stars of the Galactic disk, the project has found 219 planetary transit candidates (Udalski *et al.* 2002abc, 2008, Pont *et al.* 2008), of which seven were confirmed as planets (Konacki *et al.* 2003ab, Pont *et al.* 2004, 2008, Bouchy *et al.* 2004, Udalski *et al.* 2008). By announcing the first exoplanet discovered using the transit technique and confirmed through radial velocity measurements – OGLE-TR-56b, OGLE paved the way for extremely fruitful ground-based surveys for transiting exoplanets, such as WASP (Pollacco *et al.* 2006), HATNet (Bakos *et al.* 2004), NGTS (West *et al.* 2016) and space missions, like Kepler (Borucki *et al.* 2010) and TESS (Ricker *et al.* 2015). However, the majority of exoplanetary surveys are limited to bright nearby stars. Only the Kepler mission was capable of discovering transiting planets around distant stars, up to 1 kpc away. This ability led to significant differences when compared to results from surveys with a smaller distance range, such as those using the radial velocity method (which primarily detects planets at distances up to 100 pc). In particular, there is a difference in the occurrence rate of hot Jupiters orbiting nearby stars (Cumming *et al.* 2008, Mayor *et al.* 2011) and distant stars (Howard *et al.* 2012, Guo *et al.* 2017). Discovering transiting planets around faint stars in microlensing survey data offers a unique opportunity to investigate short orbital period planets across a wide range of galactocentric distances.

Over its more than three decades of operation, the OGLE survey has had a profound impact on many fields of modern astrophysics. In this study, we present a large sample of high-probability transiting planet candidates selected from the OGLE survey database. This database has not been searched for planetary transits since the early 2000s. The analyzed data were collected between 2010 and 2019 and consist of between 11 and 17 thousand measurements per object. Such long, regular, high-quality, and homogeneous observations have not been matched by any other survey capable of detecting transiting exoplanets.

In Section 2, we provide a brief description of the OGLE survey and the ana-

*exoplanet.eu

lyzed photometric observations. Section 3 introduces the steps taken to find, verify, and characterize planetary candidates. In Section 4, we present the final catalog of candidates. The discussion in Section 6 includes our thoughts on the future of our targets. Finally, in Section 7, we summarize our work.

2. The OGLE survey

The primary objective of the OGLE survey is a continuous monitoring of billions of stars within the Galactic bulge, disk, and the Magellanic Clouds to study their photometric variability. For this purpose, the survey employs a 32-detector mosaic camera attached to the 1.3-m Warsaw telescope at the Las Campanas Observatory, Chile, which is operated by the Carnegie Institution for Science. The installation of this camera in March 2010 marked the commencement of the OGLE’s fourth phase (Udalski *et al.* 2015). The camera has a field of view of 1.4 deg^2 and a resolution of $0.26 \text{ arcsec}/\text{px}$. The exceptional observing conditions at Las Campanas allow OGLE to collect photometric data from some of the most densely populated regions of the sky with very high precision. For our analysis, we used data from ten observational seasons, between 2010–2019. Due to the COVID-19 pandemic restrictions, OGLE temporarily stopped its regular operations in March 2020, resuming observations in August 2022. The majority of observations were taken through the Cousins I filter, with additional data collected using the Johnson V filter. For our studies, we chose four of the most frequently observed fields in the direction of the Galactic bulge, with up to 16 800 data points per object and a cadence as short as 19 min (see Table 1). The exposure times of those observations were 100 s in I and 150 s in V . The photometric data was reduced using the Difference Image Analysis (DIA, Woźniak 2000), a technique developed specifically for dense stellar fields (Alard and Lupton 1998).

Table 1
OGLE-IV fields searched for transiting planets

OGLE field	N_{obs}	$N_*(I \leq 15.5, (V - I) \leq 2)$
BLG501	15 700	29 600
BLG504	11 100	23 200
BLG505	16 800	52 600
BLG512	14 500	116 700
SUM		222 100

We focused our search on bright main-sequence stars in the Galactic disk by employing the following criteria for brightness and color selection: $I \leq 15.5$ mag and $(V - I) \leq 2$ mag. This is illustrated in Fig. 1. In total, approximately 222 100

objects within the analyzed fields met these criteria (Table 1). After reviewing the light curve of the known planetary transit OGLE-TR-10 (Udalski *et al.* 2002a) detrended with various methods, we opted for a straightforward correction method using the median value from each season. This corrects, in a sufficient way, the decrease in brightness, caused by the proper motions shifts of targets with respect to the reference images. To minimize the effects of cosmic rays, weather conditions, bad CCD columns, satellite and asteroid flybys, and other factors, we implemented a sigma clipping technique, excluding data points exceeding 2σ above the normalized flux.

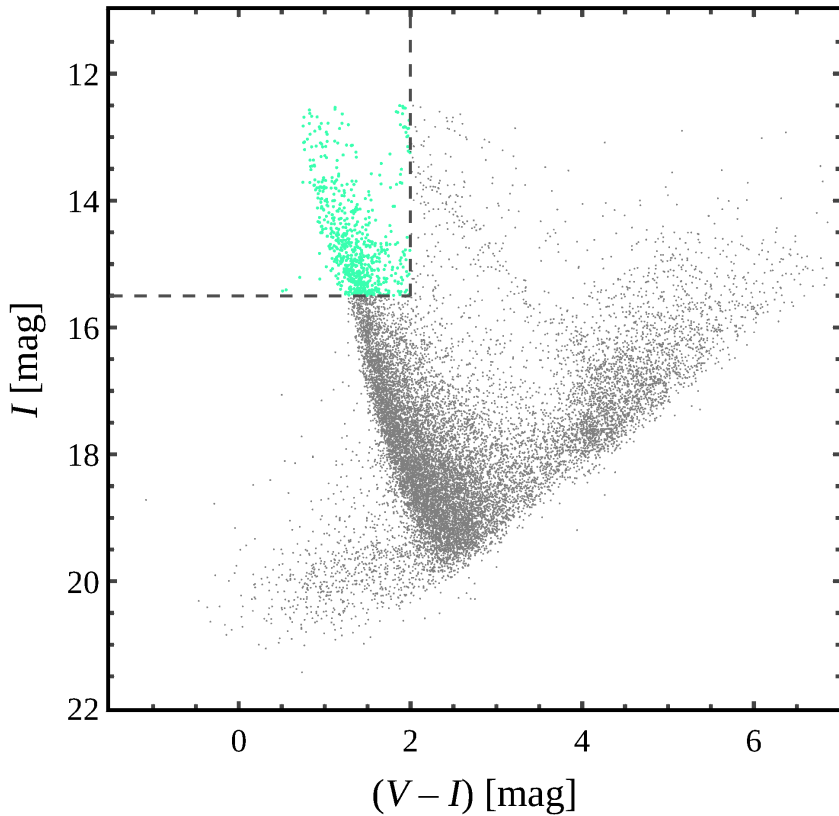


Fig. 1. Color-magnitude diagram for the OGLE sub-field BLG501.15, with the marked selection cuts.

3. Transit Detection

3.1. Initial Transits Search

A commonly used technique for transit searches involves the least squares fitting of transit templates to the light curves, folded according to a grid of trial periods. In our work, we applied the Transit Least Squares (TLS) algorithm (Hippke and Heller 2019). This modern method implements a more realistic transit shape compared to the rectangular template used in the traditional Box Least Squares (BLS) algorithm (Kovács *et al.* 2002). By including limb darkening and the planetary ingress and egress effects in the shape of the light curve, TLS is more sensitive to low signal-to-noise ratio (SNR) transits. The TLS template is based on the transit model of Mandel and Agol (2002), with parameters optimized based on a set of previously known exoplanet transit detections. The use of realistic templates increases the detection efficiency by 5-10 percent at the expense of computational speed (Hippke and Heller 2019).

Ground-based observations, such as the ones collected by the OGLE project, present additional challenges in the detection of periodic signals compared to continuous data collected by space telescopes. Various natural phenomena, like the day-night cycle, moonlight contamination, etc., can produce periodic changes in the structure of observational data (*e.g.*, Baluev 2012). To minimize false positive signals caused by these phenomena, we added an option to TLS to exclude problematic sections of tested periods from the period grid. We conducted a trial search to determine which periods should be excluded and which TLS parameters would be most suitable for our purposes. We initiated the search by excluding the most prominent multiples of the sidereal day. Subsequently, throughout this trial run, we extended the excluded period ranges to minimize recurring false positive signals. This increased the sensitivity to transit signals and reduced the TLS calculation time (final excluded period ranges are listed in Table 2). After the preliminary run, we fixed the following parameters: oversampling factor = 4, transit duration grid step = 1.1, minimum period = 0.6 d, and maximum period = 500 d. For the definition of the parameters and other details of the TLS, we refer to Hippke and Heller (2019).

Due to residual contamination, we decided to visually inspect the results of the TLS calculations for almost all the objects. We automatically excluded only signals caused by breaks in the folded data or no signal detections. True signals were classified into the following groups: transits, sinusoidal variations, and other variability. In the next step, we double-checked all the signals classified as transits to exclude obvious eclipsing binary systems (based on transit depth and the presence of a secondary eclipse). After this process, we were left with 4601 potential planetary-like transits.

Table 2

Period ranges excluded from the TLS search grid.

Excluded period range	Comment
0.6640 – 0.6665	2/3 sidereal day
0.7474 – 0.7475	3/4 sidereal day
0.990 – 1.010	1 sidereal day
1.329 – 1.331	4/3 sidereal day
1.493 – 1.499	3/2 sidereal day
1.661 – 1.664	5/3 sidereal day
1.988 – 2.001	2 sidereal day
2.492 – 2.497	5/2 sidereal day
2.981 – 3.002	3 sidereal day
3.988 – 3.9905	4 sidereal day
3.4895 – 3.490	7/2 sidereal day
4.985 – 4.9875	5 sidereal day
5.9825 – 5.984	6 sidereal day
6.980 – 6.982	7 sidereal day
54.678 – 55.180	unknown
58.603 – 58.604	unknown
64.929 – 65.931	unknown
68.410 – 68.412	unknown
100.058 – 100.062	unknown
115.205 – 115.210	unknown
146.130 – 146.140	unknown

3.2. Probabilistic Evaluation

The major disadvantage of the transit method is the need for additional confirmation of the planetary nature of transiting objects. Firstly, from the shape of the transit, we can only deduce the radius of the transiting object. Therefore, we cannot distinguish between hot Jupiters, brown dwarfs, and low-mass M-type stars, as they can all have similar sizes. Secondly, additional light blended in the photometric aperture can shallow the transit depth and lead to underestimated radius measurements. The traditional way of resolving this degeneracy is to measure the mass through radial velocity (RV) observations. Nevertheless, there are indirect methods of validation in the absence of RV measurements. One of them is the Validation of Exoplanet Signals using a Probabilistic Algorithm (VESPA, Morton 2012). VESPA is a widely used and well-established publicly available software package that performs statistical validation. We used it to evaluate 4601 candidates against astrophysical false positive scenarios. By applying a simple trapezoidal transit model, known parameters of the host star, and assumptions about the popu-

lations and distribution of field stars, the algorithm calculates the probability of the analyzed object being a planet given the observed signal $\text{Pr}(\text{planet}|\text{signal})$. VESPA considers the following false positive scenarios:

- blended eclipsing binary (BEB), in the case of non-associated eclipsing binary systems blended within the photometric aperture of the target star,
- hierarchical eclipsing binary (HEB), in case of the target is a hierarchical triple system in which two components are eclipsing,
- eclipsing binary (EB).

For detailed descriptions, we refer to Morton (2012, 2016).

We prepared normalized flux light curves in the same way as for the TLS. As initial values required by VESPA (the orbital period P , planet-to-star radius ratio R_p/R_*), we used values fitted by the TLS. We derived the maximum allowed depth of a potential secondary eclipse for each object by searching the phase-folded light curve for the deepest signal at any phase outside of the primary transit (Morton 2016). We set the maximum angular distance (parameter *maxrad* in VESPA) from the target star where a potential blending star might be, as $2''.6$, which is 10 times the pixel size of the OGLE-IV camera or roughly twice the average seeing of the images.

The obtained values of probability for the planetary origin of transits are shown in the histogram in Fig. 2. For further analysis, we decided to use only the cases for which the probability is greater than 80%. Scenarios with the highest probability for each analyzed transit are shown in Fig. 3. For 1110 transits, VESPA calculation failed, in most cases due to not converging transit model.

3.3. Modeling the Candidates

We chose EXOFASTv2 (Eastman *et al.* 2019) for modeling our candidates, which is Markov Chain Monte Carlo (MCMC) transit modeling code. To properly model the transit, it is essential to model both the host star and the planet. EXOFASTv2 offers the unique capability of simultaneously constraining host star parameters using both the transit shape and stellar models, employing isochrones from stellar evolutionary tracks and spectral energy distribution (SED). These features of the code are particularly helpful in constraining system parameters, especially when spectroscopic observations are unavailable.

For modeling, we used OGLE observations in both the *I*- and *V*-bands, which were detrended and normalized as in previous steps. When an object was observed in multiple OGLE fields, we added those observations as separate data sets. In a few cases, this notably enlarged the number of observations, as for example for OGLE-TR-1051 (see Fig. 10). We converted the original OGLE time stamps from Heliocentric Julian Date (HJD) to Barycentric Julian Date (BJD_{TDB}) using IDL codes written by Eastman (2010). As starting values for the period P_{orb} and the time of

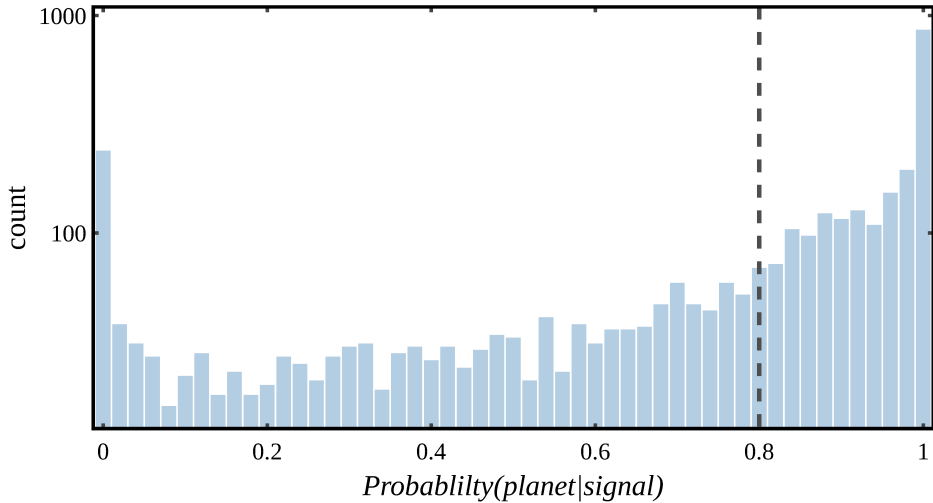


Fig. 2. Distribution of $\text{Pr}(\text{planet}|\text{signal})$ values for 3491 potential planetary-like transit. The dashed line marks the minimum value of the probability for which transit was used in further analyzes.

conjunction T_C , we implemented values from the TLS output. Whenever available, we incorporated parallax ϖ and host effective temperature T_{eff} values from Gaia DR3 (Gaia Collaboration *et al.* 2023a). We applied upper limits for interstellar extinction toward the Galactic bulge, as calculated by Nataf *et al.* (2013). In only a few cases, we utilized Galactic extinction maps by Gonzalez *et al.* (2012). SED modeling requires measurements of the star's bolometric flux in various bands. We reviewed publicly available photometric catalogs and their reference images for the Galactic bulge region. As a test case, we used the well-characterized planetary system OGLE-TR-10 (Udalski *et al.* 2002a, Konacki *et al.* 2003b, Melo *et al.* 2006), which is located in one of the analyzed fields, and its transit was detected in the TLS search. For this object, we prepared a set of modeling inputs in the same manner as for our candidates. Following SED modeling of OGLE-TR-10, we compared the fitted parameters to those reported in the literature. Ultimately, we decided to use measurements from the Dark Energy Camera Plane Survey 2 (DECaPS2, Saydjari *et al.* 2023), the Pan-STARRS1 Surveys DR2 (Chambers *et al.* 2016), and synthetic photometry from the Gaia DR3 low-resolution spectra (Gaia Collaboration *et al.* 2023b), as this set resulted in the best agreement between calculated parameters and those reported from high-resolution spectroscopy. We assumed circular orbits for all of our objects since they are on short-period orbits. For stellar evolution models, we selected the default in EXOFASTv2 - the MESA Isochrones and Stellar Tracks (MIST) model (Choi *et al.* 2016). For each object, we performed a preliminary short modeling with parallel tempering. Subsequently, using the preliminary results, we recreated priors and conducted final modeling without parallel tempering and with 50 000 maximum steps.

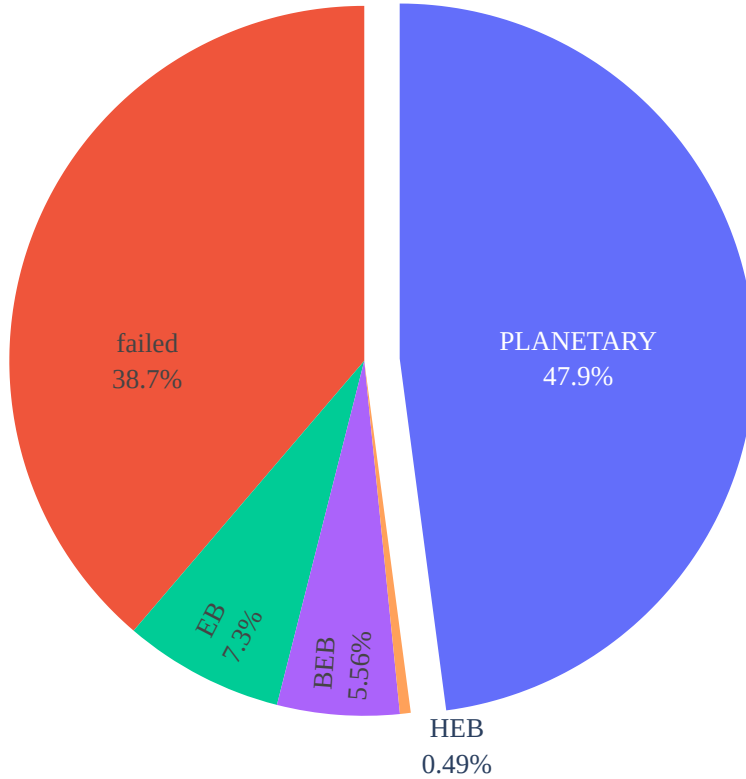


Fig. 3. Most probable scenario for 4601 potential planetary-like transits. Each slide represents a different scenario simulated with VESPA: BEB – blended eclipsing binary, HEB – hierarchical triple system with eclipse, EB – eclipsing binary. PLANETARY – planetary transits, failed – VESPA calculations failed.

3.4. Final Selection

To further reduce the likelihood of false positive signals in our catalog, we conducted additional tests on all objects for which we successfully created models. Our aim was to ensure that the transit signal in the light curve was not an artifact of a nearby eclipsing binary system. To achieve this, we cross-matched our candidates with the OGLE collection of eclipsing and ellipsoidal binary systems (Soszyński *et al.* 2016). Within 1' radius around each candidate, we examined if there was a binary system with an orbital period or its alias consistent with that of our candidate. If such a match was found, we excluded the object from further analysis. This was the case for 138 out of 1243 transits at this stage of the vetting process. In the same manner as for the binary systems catalog, we cross-matched our final candidates with all the results from the TLS search. This additional step was designed to help

eliminate false positive signals of instrumental origin and resulted in the exclusion of additional 110 detections. Furthermore, we analyzed the histogram of periods detected by the TLS in each observed field and removed candidates with orbital periods close to the peaks of this histogram. An example section of the histogram from field BLG501 is shown in Fig. 4. Those peaks vary between observation fields and can be associated with multiple astrophysical or instrumental signals, such as remaining aliases of the sidereal day, diffraction spikes from nearby bright stars, lunar cycle, or bad columns in the CCD detector. We checked previously reported planetary-like transits from the third phase of the OGLE project (Udalski *et al.* 2002abc, 2008, Pont *et al.* 2008), and we did not find any matches with our detections beside the mentioned OGLE-TR-10. OGLE-TR-10b is the only confirmed planet, which was regularly observed during OGLE-IV. The absence of matches with previously unconfirmed candidates can be attributed to the more rigorous selection process.

To conclude the selection process, we chose the 99 most promising candidates for transiting planets, which will be presented in detail in Section 4. This final step considered various factors, including the number of observations, how well the created model fits the observational data, and whether the transit exhibits the V-shape, which could indicate a grazing binary system eclipse.

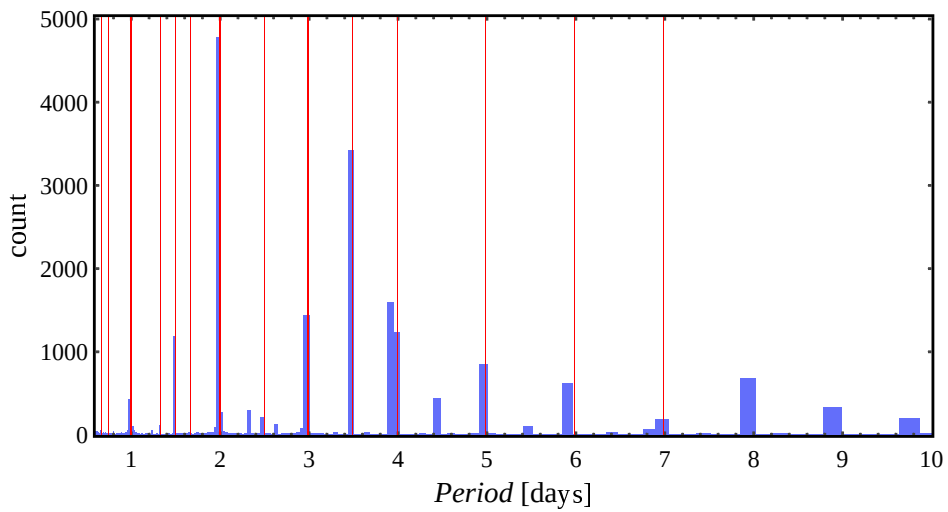


Fig. 4. Example section of the orbital periods distribution resulting from the TLS search in the field BLG501. Each bin represents 2000 values from the TLS period grid. The red fields indicate the excluded periods from Table 2.

4. The Planetary Candidates

Here, we present the selected planetary candidates. Table 3 displays their observational parameters, including celestial coordinates, orbital period of the companion (P_{orb}), time of conjunction (T_c), total transit duration (T_{14}), fractional transit depth (δ), brightness in I - and V -band, signal-to-noise ratio (SNR), and the probability that the transit is of planetary origin given the signal ($\text{Pr}(\text{planet}|\text{signal})$). Table 4 presents the selected physical parameters of the systems, including parameters of the host such as mass (M_*), radius (R_*), surface gravity ($\log g$), effective temperature (T_{eff}), metalicity ([Fe/H]), and distance (d); parameters of the companion such as orbital radius (a), inclination (i), and equilibrium temperature (T_{eq}). For the detailed definitions of the parameters, we refer to Eastman *et al.* (2019). Figs. 7-13 show observational data of transits with fitted models. The identifiers of our planetary candidates follow the format OGLE-TR-NNNN, where NNNN represents a four-digit consecutive number starting from 1001 to distinguish from previous findings of the OGLE project (Udalski *et al.* 2002abc, 2008, Pont *et al.* 2008). The SNR is defined as:

$$\text{SNR} = \frac{\delta}{\sigma_o} n^{1/2} \quad (1)$$

where δ represents the transit depth, σ is the standard deviation of the out-of-transit points, and n is the number of in-transit points (Pont *et al.* 2006). Calculations of SNR values are based on EXOFASTv2 models. All the selected candidates have SNR greater than 6, with median value $\text{med}(\text{SNR}) = 20.46$. The values of probability that the transit is of planetary origin $\text{Pr}(\text{planet}|\text{signal})$ were obtained with VESPA. As mentioned above, $\text{Pr}(\text{planet}|\text{signal})$ ranges between 0.8 and 1.0, with $\text{Pr}(\text{planet}|\text{signal}) \geq 0.99$ for 63 objects. The remaining parameters are median values resulting from the MCMC modeling (for detailed definitions of the parameters see Eastman *et al.* 2019). The majority of our candidates belong to the hot Jupiters family. The orbital periods range from 0.67 d (slightly above the minimal period search by the TLS algorithm, 0.60 d) to 63.22 d. The radii of companions are typical for Jupiter-like gas giants, with a median value of $\text{med}(R_p) = 1.385 R_J$, with an exception of OGLE-TR-1003b. This candidate has the size corresponding to Neptune-like planets ($R_p = 0.529 R_J$). The proximity to its host star places OGLE-TR-1003b in the parameter space of the so-called hot Neptune desert, which is an observed dearth of Neptune-size planets on orbits with periods shorter than $\approx 5 - 10$ d (Mazeh *et al.* 2016). In Fig. 5 we present how the radii of candidates are distributed depending on the orbital period or equilibrium temperature, with the Neptune desert area marked. The distance distributions of the candidates span between 0.4 kpc and 5.5 kpc, which translates to 2.8 – 7.9 kpc from the Galactic center, as shown in Fig. 6. Additionally, Fig. 6 illustrates the uniqueness of our findings in comparison to other known exoplanets in the Galaxy. To date, only observations from the Hubble Space Telescope have enabled

the detection of sixteen transiting planetary candidates (two confirmed through RV measurements) close to the Galactic center (Sahu *et al.* 2006, 2008). The only detection method that efficiently probes this region of the Galaxy is the microlensing method. Nevertheless, this method is sensitive to planets on wider orbits compared to transit detections and, due to its transient nature, limits follow-up in-depth characterization of systems.

The full list of determined parameters of the systems with photometric data is available on the OGLE website [†].

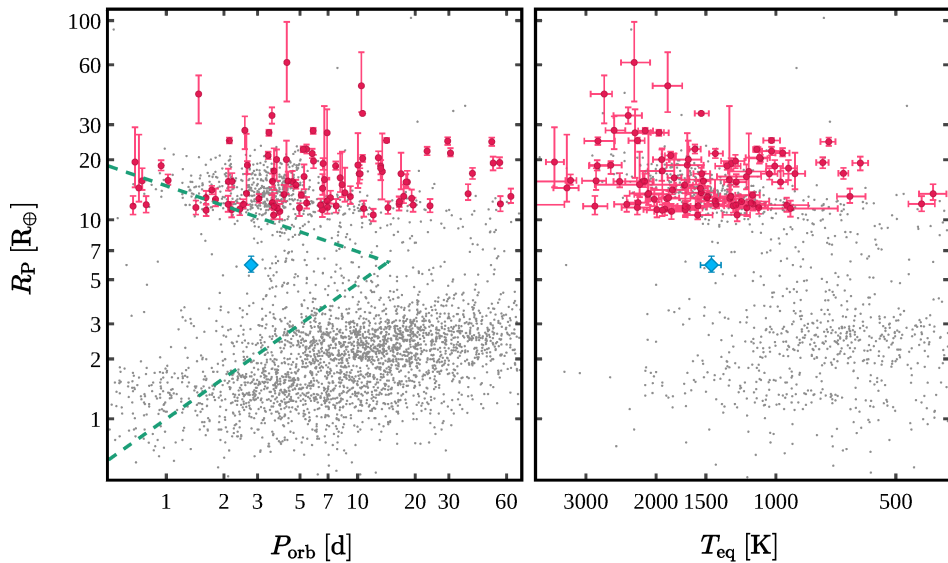


Fig. 5. Parameters of detected planetary candidates. The Jovian-size objects are indicated by red points with error bars. Blue diamond mark the sub-Jovian object – OGLE-TR-1003. Gray dots – currently known confirmed planets (exoplanets.eu, as for September 2023). The hot Neptune desert from Mazeh *et al.* (2016) shown with dashed lines in the left panel.

[†]ogledb.astroww.edu.pl/~ogle/OCVS/

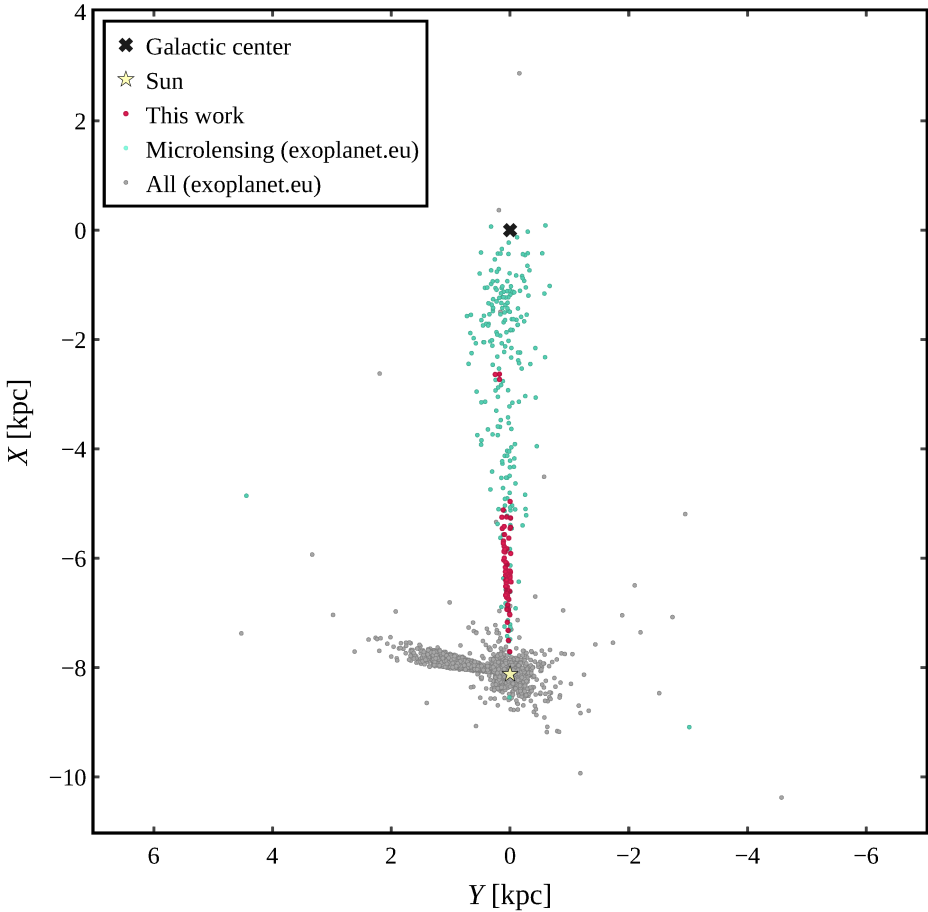


Fig. 6. Galactic distribution of our planetary candidates and known confirmed exoplanets (exoplanets.eu, as for September 2023).

5. Future Prospects

We confirmed that observations of the Galactic bulge regions offer opportunities for planetary transit research. These regions are often overlooked by typical transit surveys due to the challenges associated with crowding. Nevertheless, they are and will continue to be monitored by surveys with a specific focus on detecting microlensing events. The large number of photometric measurements collected this way can be used for planetary transit studies.

One of the notable advantages of our catalog is the extended time span of available observations. For many of our candidates, we can expand the time coverage to an exceptional 23-year period by incorporating observations from the previous phase of the OGLE project (OGLE-III, 2001-2009). This long time span of reg-

ular observations has not been achieved by any other survey capable of detecting exoplanets. Consequently, our planetary candidates become valuable objects for studies of long-term orbital evolution (Hagey *et al.* 2022).

Furthermore, the upcoming Nancy Grace Roman Space Telescope (Spergel *et al.* 2015, Montet *et al.* 2017) is expected to provide an additional 40 000 precise photometric and astrometric measurements of our targets. While our objects are brighter than the planned saturation limit of Roman (14.8 mag in filter *W149*, Penny *et al.* 2019), the expected relative precision will still be of order of 1 part per thousand (Montet *et al.* 2017). Using noise estimation for a single epoch in the Roman *W149* filter from Gould *et al.* (2015):

$$\sigma = 1.0 \times 10^{(2/15)(H-15)} \text{ mmag} \quad \text{for } 8 \lesssim H \lesssim 15 \text{ mag} \quad (2)$$

where H stands for the near-infrared H -band, using values determined from created SED models, we find that for our targets, σ would be around 0.001 mag.

As we mentioned in Subsection 3.2, the time-series observations alone are not enough to confirm the planetary nature of the objects. Given the relative faintness of our targets and the accessibility of telescopes, performing follow-up RV observations for all our candidates may not be achievable. Nevertheless, this challenge exists since transit detections have increased in numbers, and various alternative validation methods have been developed, such as the probabilistic validation method used by us. Conducting additional photometric observations, including multi-band transit observations or high-resolution adaptive optics observations, will further help in establishing the level of blended light. Additionally, obtaining low-resolution spectroscopic observations of the host stars can help narrow down their parameters and, indirectly, the parameters of the companions.

It is important to acknowledge that many of the selection steps for candidates presented in this work were subjective. Therefore, we advise exercising caution when using this catalog beyond a collection of individual cases for further analyses.

6. Conclusions

We conducted a planetary transit search using photometric observations collected during the fourth phase of the OGLE project. We used observations of main sequence stars within four fields covering a total area of 5.6 deg² in the direction of the Galactic bulge. To identify potential candidates, we employed a method that fits realistic transit shapes to data folded according to the grid of trial periods. After the vetting process, which included the evaluation of the probability of false positive signals, we selected the most promising objects. Using all available data, sourced both from the OGLE project and the public domain, we developed comprehensive models of planetary systems. We presented selected 99 highly-probable planetary candidates. The majority of these candidates fall within the category of hot and warm Jupiters, with the exception of one object exhibiting a sub-Jovian

size. Notably, this companion in OGLE-TR-1003 is located in the hot Neptune desert. Our candidates are distributed across a wide range of distances, extending up to 5.5 kpc, dovetailing with planets discovered with the microlensing method. This synergy offers an extraordinary opportunity for the study of planetary systems, encompassing those with the shortest to the longest orbital periods as a function of Galactic distance. Furthermore, finding transiting planets in fields monitored by microlensing surveys is extremely beneficial in terms of time coverage of observations. In the case of our candidates, the OGLE database can provide regular and consistent observations since 2001, with the potential for further extensions as the project continues. Additionally, the upcoming Nancy Grace Roman Space Telescope mission is expected to provide additional observations of our targets with improved precision.

Acknowledgements. We thank all the OGLE observers for their contribution to the collection of the photometric data over the decades.

This work has been funded by the National Science Centre, Poland, grant no. 2022/45/B/ST9/00243. For the purpose of Open Access, the author has applied a CC-BY public copyright license to any Author Accepted Manuscript (AAM) version arising from this submission.

We used data from the European Space Agency (ESA) mission Gaia, processed by the Gaia Data Processing and Analysis Consortium (DPAC). Funding for the DPAC has been provided by national institutions, in particular the institutions participating in the Gaia Multilateral Agreement.

This project used public archival data from the Dark Energy Survey (DES). Funding for the DES Projects has been provided by the U.S. Department of Energy, the U.S. National Science Foundation, the Ministry of Science and Education of Spain, the Science and Technology Facilities Council of the United Kingdom, the Higher Education Funding Council for England, the National Center for Supercomputing Applications at the University of Illinois at Urbana-Champaign, the Kavli Institute of Cosmological Physics at the University of Chicago, the Center for Cosmology and Astro-Particle Physics at the Ohio State University, the Mitchell Institute for Fundamental Physics and Astronomy at Texas A&M University, Financiadora de Estudos e Projetos, Fundação Carlos Chagas Filho de Amparo à Pesquisa do Estado do Rio de Janeiro, Conselho Nacional de Desenvolvimento Científico e Tecnológico and the Ministério da Ciência, Tecnologia e Inovação, the Deutsche Forschungsgemeinschaft, and the Collaborating Institutions in the Dark Energy Survey. The Collaborating Institutions are Argonne National Laboratory, the University of California at Santa Cruz, the University of Cambridge, Centro de Investigaciones Energéticas, Medioambientales y Tecnológicas-Madrid, the University of Chicago, University College London, the DES-Brazil Consortium, the University of Edinburgh, the Eidgenössische Technische Hochschule (ETH) Zürich, Fermi National Accelerator Laboratory, the University of Illinois at Urbana-

Champaign, the Institut de Ciències de l’Espai (IEEC/CSIC), the Institut de Física d’Altes Energies, Lawrence Berkeley National Laboratory, the Ludwig-Maximilians Universität München and the associated Excellence Cluster Universe, the University of Michigan, the National Optical Astronomy Observatory, the University of Nottingham, The Ohio State University, the OzDES Membership Consortium, the University of Pennsylvania, the University of Portsmouth, SLAC National Accelerator Laboratory, Stanford University, the University of Sussex, and Texas A&M University. Based in part on observations at Cerro Tololo Inter-American Observatory, National Optical Astronomy Observatory, which is operated by the Association of Universities for Research in Astronomy (AURA) under a cooperative agreement with the National Science Foundation.

The Pan-STARRS1 Surveys (PS1) and the PS1 public science archive have been made possible through contributions by the Institute for Astronomy, the University of Hawaii, the Pan-STARRS Project Office, the Max-Planck Society and its participating institutes, the Max Planck Institute for Astronomy, Heidelberg and the Max Planck Institute for Extraterrestrial Physics, Garching, The Johns Hopkins University, Durham University, the University of Edinburgh, the Queen’s University Belfast, the Harvard-Smithsonian Center for Astrophysics, the Las Cumbres Observatory Global Telescope Network Incorporated, the National Central University of Taiwan, the Space Telescope Science Institute, the National Aeronautics and Space Administration under Grant No. NNX08AR22G issued through the Planetary Science Division of the NASA Science Mission Directorate, the National Science Foundation Grant No. AST-1238877, the University of Maryland, Eotvos Lorand University (ELTE), the Los Alamos National Laboratory, and the Gordon and Betty Moore Foundation.

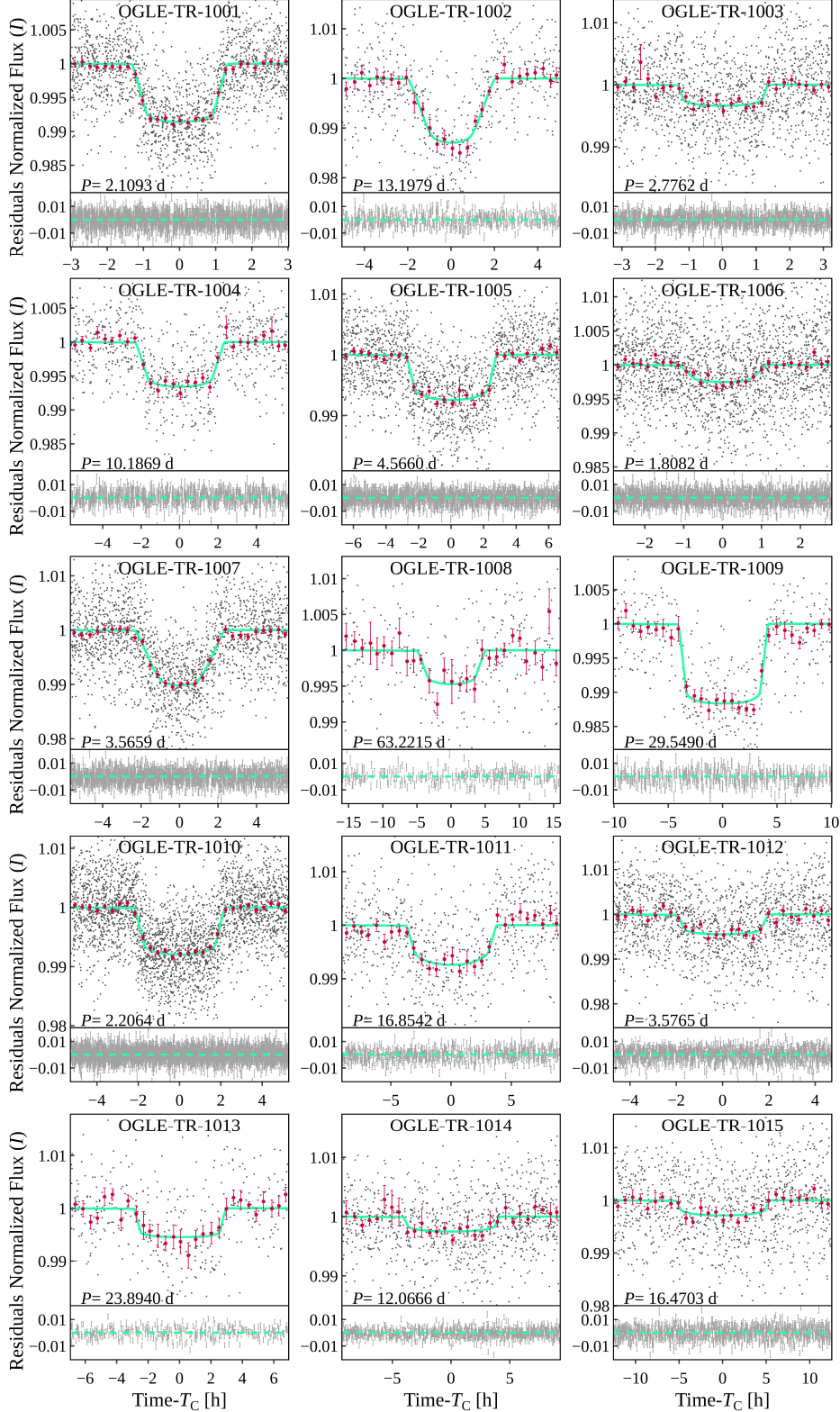


Fig. 7. Light curves of planetary transit candidates: OGLE-TR-1001–OGLE-TR-1015. Gray points – folded observational data, red points – binned observational data, green line – fitted MCMC model with minima χ^2 .

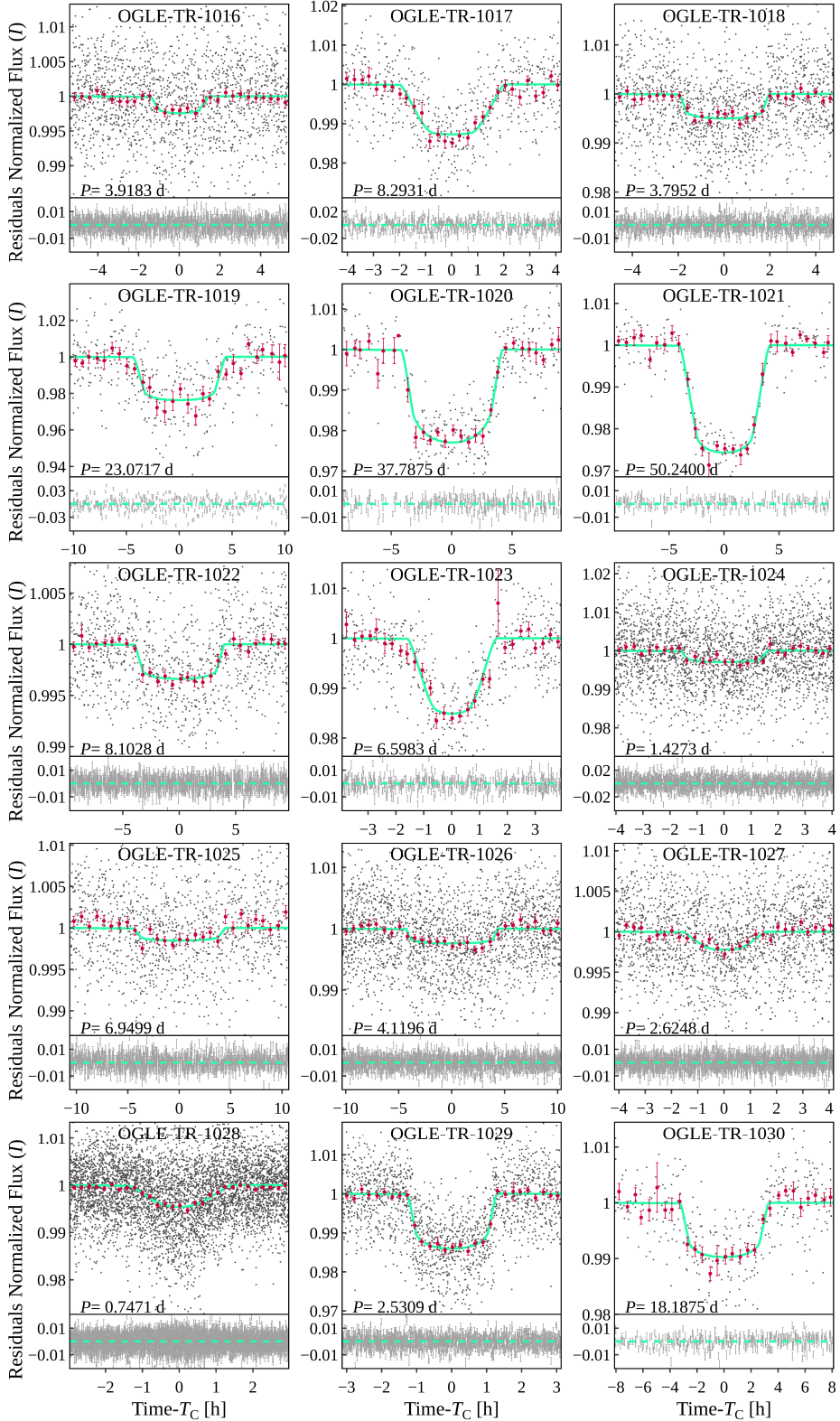


Fig. 8. Same as Fig. 7, planetary transit candidates: OGLE-TR-1016–OGLE-TR-1030.

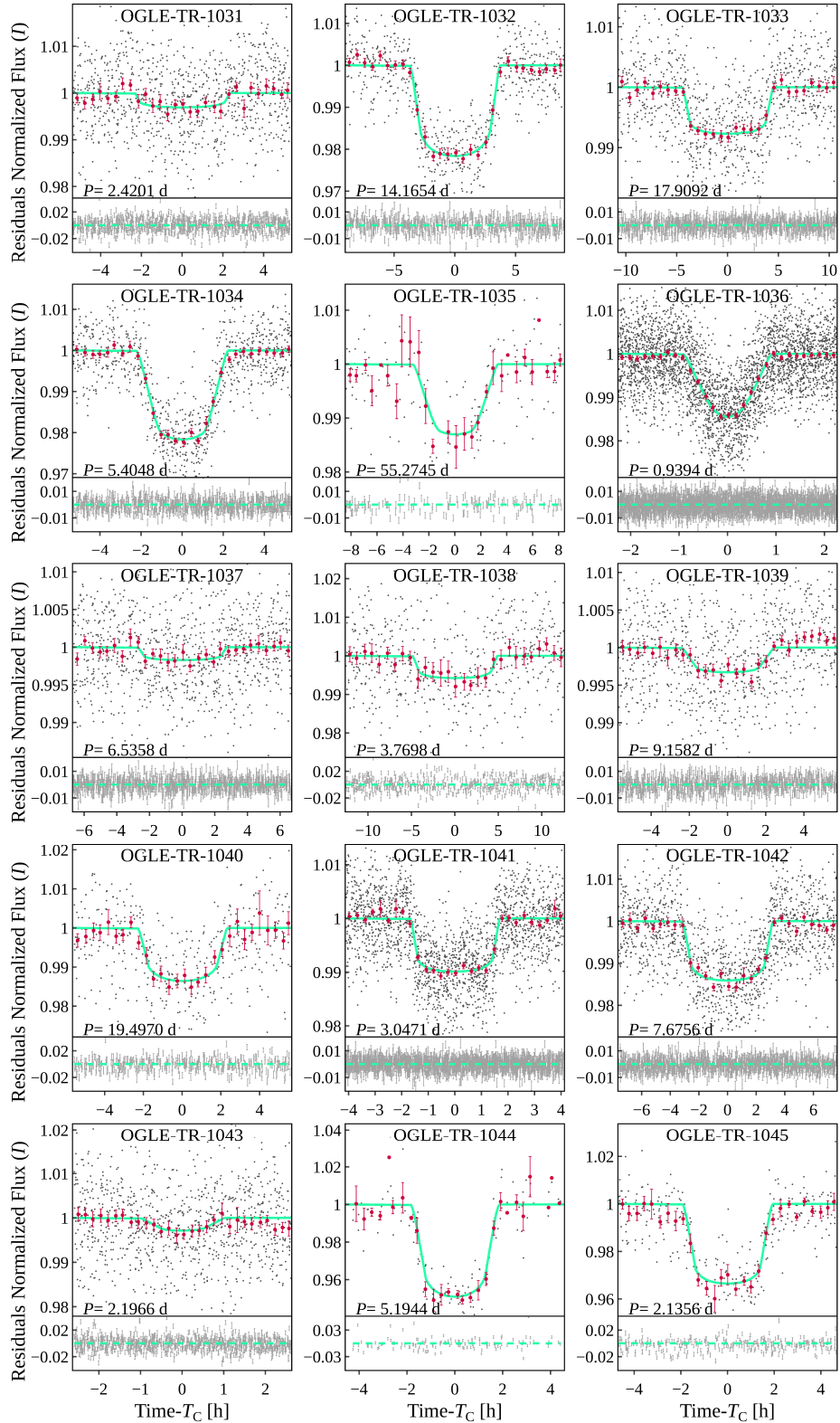


Fig. 9. Same as Fig. 7, planetary transit candidates: OGLE-TR-1031–OGLE-TR-1045.

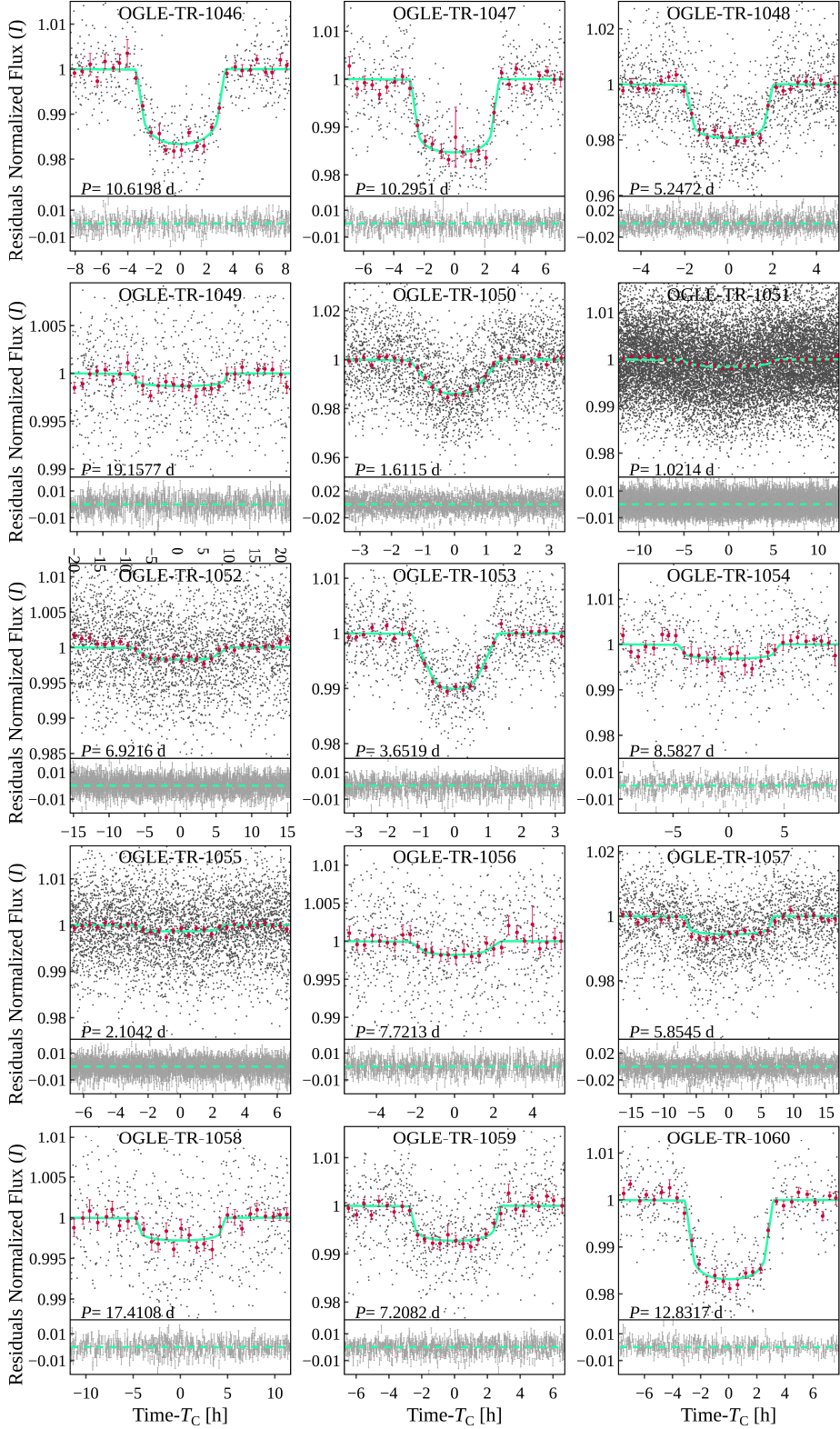


Fig. 10. Same as Fig. 7, planetary transit candidates: OGLE-TR-1046–OGLE-TR-1060.

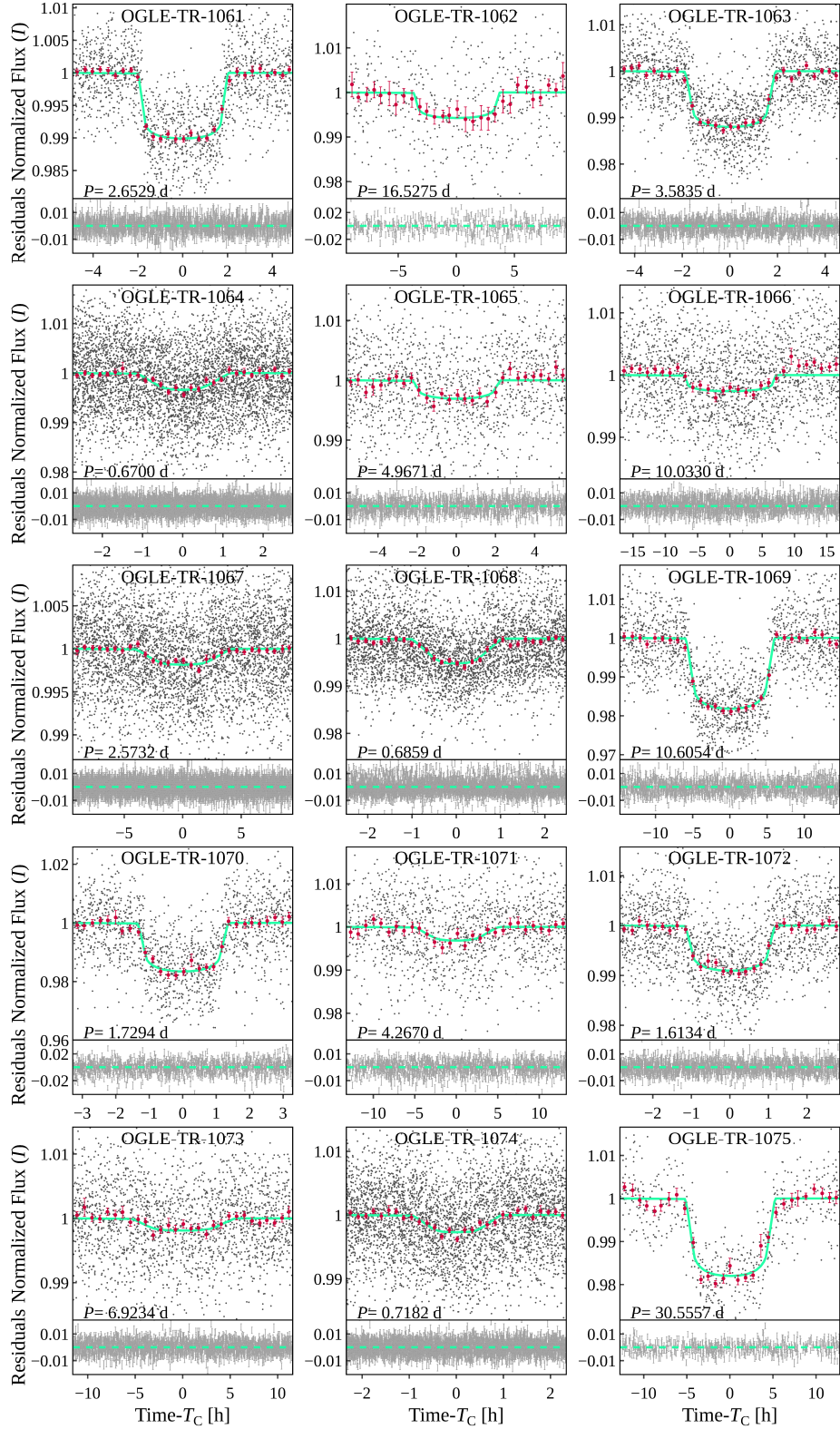


Fig. 11. Same as Fig. 7, planetary transit candidates: OGLE-TR-1061–OGLE-TR-1075.

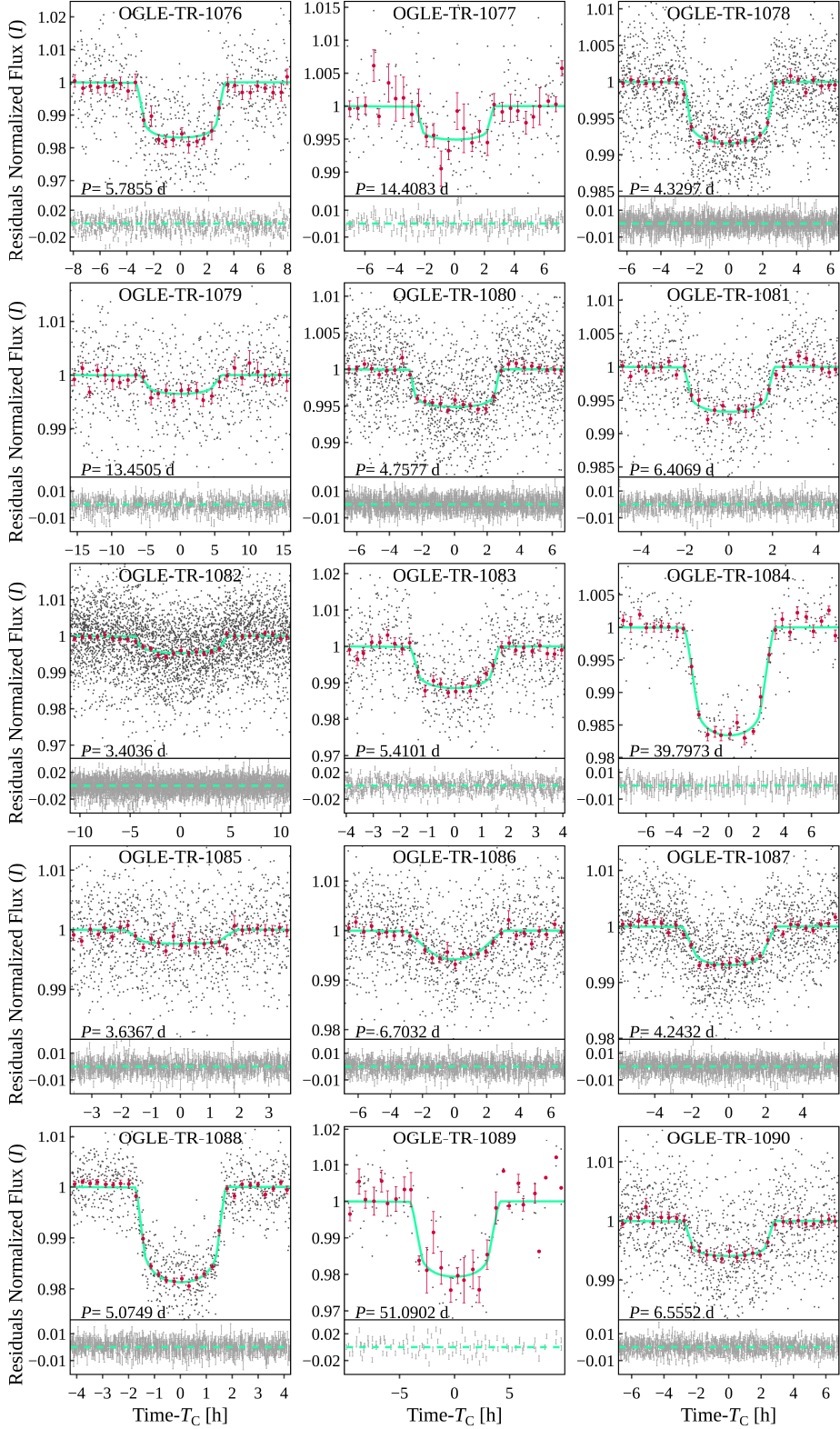


Fig. 12. Same as Fig. 7, planetary transit candidates: OGLE-TR-1076–OGLE-TR-1090.

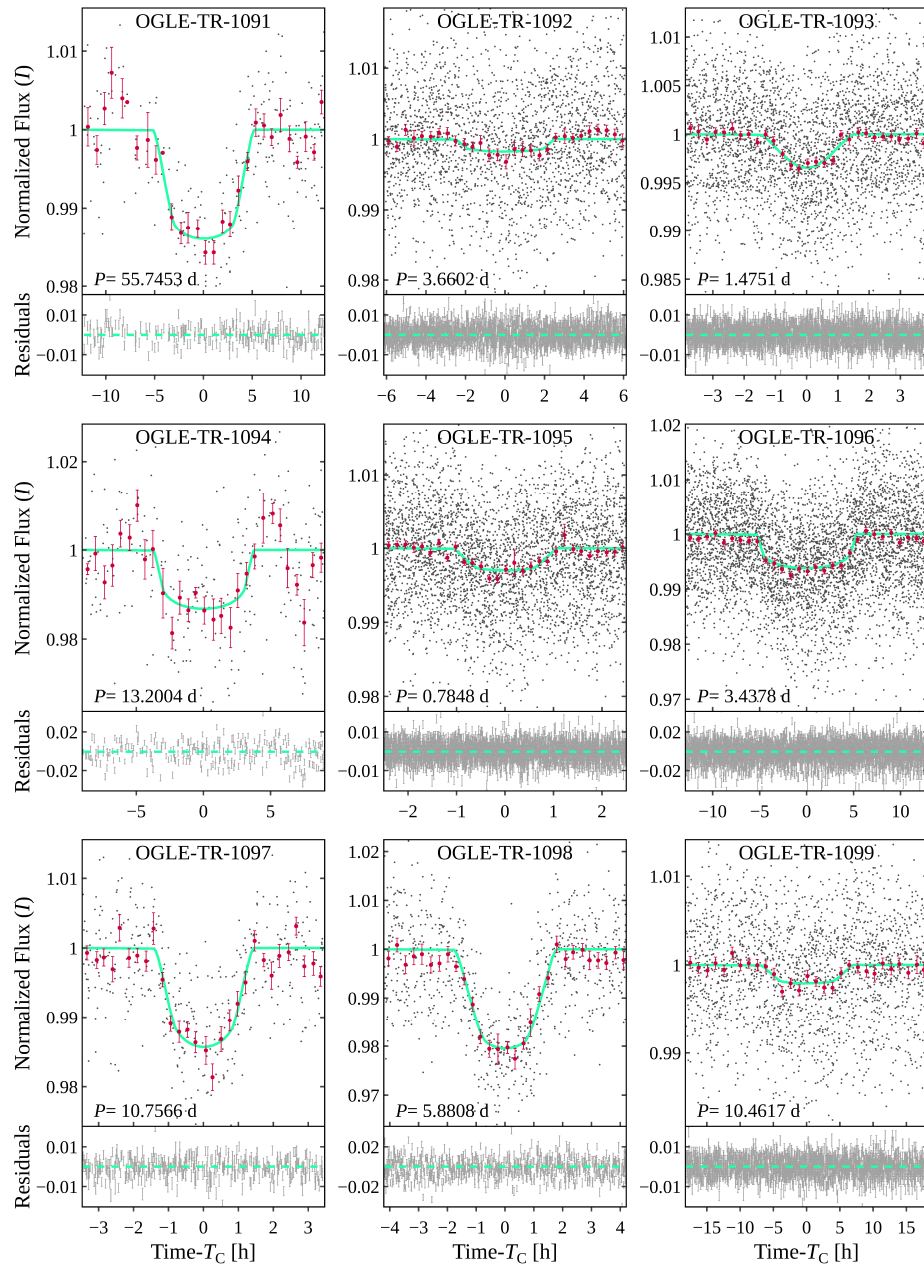


Fig. 13. Same as Fig. 7, planetary transit candidates: OGLE-TR-1091–OGLE-TR-1099.

Table 3
Observational parameters of systems with planetary candidates.

Name	RA (J2000)	DEC (J2000)	P_{orb} [d]	T_c [BJD _{TDB} − 2450000]	T_{14} [d]	δ	I [mag]	V [mag]	SNR	Pr(planet signal)
OGLE-TR-1001	17 : 49 : 43.17	−29 : 23 : 41.9	2.1093174	5378.18379	0.1043	0.00823	13.923	14.815	58.05	1.00
OGLE-TR-1002	17 : 49 : 51.28	−29 : 18 : 01.1	13.197893	5379.7864	0.1740	0.0142	15.419	17.021	32.86	0.93
OGLE-TR-1003	17 : 50 : 22.77	−29 : 23 : 19.4	2.7762253	5379.3403	0.1123	0.00285	15.382	16.872	12.60	1.00
OGLE-TR-1004	17 : 50 : 23.35	−30 : 15 : 01.4	10.186892	5379.8420	0.1964	0.00635	14.168	15.348	29.93	1.00
OGLE-TR-1005	17 : 50 : 28.70	−29 : 54 : 23.9	4.5659828	5380.5474	0.2317	0.00655	14.824	15.931	35.43	1.00
OGLE-TR-1006	17 : 50 : 38.40	−29 : 22 : 06.8	1.8082001	5377.0093	0.0970	0.00287	14.902	16.640	16.33	0.99
OGLE-TR-1007	17 : 50 : 47.56	−30 : 11 : 59.7	3.5659243	5379.2049	0.1960	0.01082	12.855	13.626	56.25	1.00
OGLE-TR-1008	17 : 50 : 48.36	−29 : 40 : 49.1	63.2215	5416.535	0.552	0.00331	15.056	16.583	6.39	1.00
OGLE-TR-1009	17 : 50 : 56.70	−29 : 40 : 49.1	29.549047	5398.1766	0.3472	0.01088	14.155	15.146	36.99	1.00
OGLE-TR-1010	17 : 51 : 30.88	−29 : 55 : 45.2	2.2063895	5377.4247	0.1826	0.00699	14.519	15.718	51.76	1.00
OGLE-TR-1011	17 : 51 : 53.22	−30 : 01 : 15.7	16.854160	5389.1759	0.313	0.00654	15.463	17.080	15.91	0.99
OGLE-TR-1012	17 : 52 : 14.08	−29 : 14 : 41.8	3.576539	5379.8131	0.1629	0.00396	15.365	16.549	14.31	1.00
OGLE-TR-1013	17 : 52 : 27.45	−29 : 53 : 02.5	23.89398	5390.170	0.240	0.00538	15.031	16.035	9.03	0.99
OGLE-TR-1014	17 : 52 : 29.08	−29 : 25 : 30.7	12.06657	5379.955	0.321	0.00254	14.280	15.423	7.05	0.98
OGLE-TR-1015	17 : 52 : 32.93	−30 : 03 : 59.9	16.47033	5377.320	0.433	0.00241	15.432	16.491	7.33	1.00
OGLE-TR-1016	17 : 52 : 47.03	−29 : 53 : 32.2	3.918334	5377.401	0.186	0.00184	15.122	16.191	8.98	0.88
OGLE-TR-1017	17 : 53 : 03.85	−30 : 06 : 36.0	8.293105	5378.3103	0.1452	0.0121	15.172	16.462	23.69	1.00
OGLE-TR-1018	17 : 54 : 28.67	−30 : 04 : 39.9	3.795212	5376.7046	0.1650	0.00446	15.380	16.568	15.26	1.00
OGLE-TR-1019	17 : 54 : 35.45	−27 : 43 : 17.3	23.07172	5377.6698	0.358	0.0215	15.306	17.194	17.85	0.92
OGLE-TR-1020	17 : 55 : 01.28	−29 : 27 : 10.0	37.78747	5388.5955	0.313	0.0202	15.348	17.030	38.64	1.00
OGLE-TR-1021	17 : 55 : 17.82	−27 : 37 : 51.7	50.24001	5394.4031	0.3439	0.02392	14.680	15.917	36.94	0.98
OGLE-TR-1022	17 : 55 : 17.87	−27 : 52 : 33.5	8.102826	5383.7016	0.335	0.00336	14.119	15.414	21.31	0.99
OGLE-TR-1023	17 : 55 : 18.63	−28 : 22 : 08.5	6.598261	5378.3482	0.1358	0.0161	15.220	16.799	36.96	1.00
OGLE-TR-1024	17 : 55 : 28.73	−27 : 26 : 23.4	1.4272776	5377.3506	0.1400	0.00269	15.145	16.774	9.66	0.94
OGLE-TR-1025	17 : 55 : 41.38	−27 : 29 : 06.8	6.949874	5377.984	0.368	0.00138	14.727	16.192	7.64	0.84

continued on next page

Table 3
Continued

Name	RA (J2000)	DEC (J2000)	P_{orb} [d]	T_c [BJD _{TDB} − 2450000]	T_{14} [d]	δ	I [mag]	V [mag]	SNR	Pr(planet signal)
OGLE-TR-1026	17 : 55 : 43.01	−27 : 55 : 57.9	4.119552	5376.948	0.357	0.00208	14.528	15.635	10.82	0.97
OGLE-TR-1027	17 : 55 : 49.63	−29 : 11 : 39.3	2.624793	5261.407	0.144	0.00203	14.785	16.199	12.84	0.82
OGLE-TR-1028	17 : 55 : 56.66	−29 : 17 : 03.8	0.74714108	5376.7574	0.1027	0.00489	13.753	15.111	43.03	0.90
OGLE-TR-1029	17 : 56 : 00.49	−28 : 49 : 24.8	2.5308880	5261.7539	0.1081	0.01217	15.194	16.400	44.07	1.00
OGLE-TR-1030	17 : 56 : 05.22	−27 : 56 : 09.0	18.187463	5388.3494	0.280	0.00841	15.276	16.945	18.11	0.99
OGLE-TR-1031	17 : 56 : 11.67	−27 : 40 : 02.7	2.420147	5376.749	0.186	0.00280	14.337	15.605	7.38	1.00
OGLE-TR-1032	17 : 56 : 16.96	−28 : 24 : 39.9	14.165438	5383.9723	0.3117	0.01825	15.242	16.913	50.46	1.00
OGLE-TR-1033	17 : 56 : 22.42	−29 : 10 : 17.1	17.909180	5381.5566	0.3724	0.00680	15.296	16.933	25.54	1.00
OGLE-TR-1034	17 : 56 : 39.10	−27 : 36 : 45.3	5.4047713	5377.5239	0.1843	0.02099	15.194	16.986	62.69	0.98
OGLE-TR-1035	17 : 56 : 42.84	−28 : 19 : 34.9	55.274448	5379.163	0.292	0.0124	13.646	14.566	15.59	0.98
OGLE-TR-1036	17 : 56 : 47.29	−28 : 37 : 15.7	0.93942100	5261.03860	0.0782	0.01648	14.029	14.911	96.27	0.92
OGLE-TR-1037	17 : 57 : 00.17	−28 : 20 : 07.3	6.535826	5381.591	0.232	0.00162	14.706	15.982	7.21	0.86
OGLE-TR-1038	17 : 57 : 12.92	−27 : 29 : 09.3	3.769846	5379.148	0.436	0.00477	13.630	14.904	6.95	1.00
OGLE-TR-1039	17 : 57 : 19.05	−29 : 49 : 41.8	9.158188	5380.9316	0.1984	0.00325	14.900	16.115	13.59	0.94
OGLE-TR-1040	17 : 57 : 21.04	−28 : 49 : 13.1	19.496967	5277.9227	0.1955	0.01203	15.394	16.719	18.42	1.00
OGLE-TR-1041	17 : 57 : 27.61	−29 : 30 : 00.4	3.0470709	5377.2418	0.1426	0.00881	14.996	16.394	45.77	1.00
OGLE-TR-1042	17 : 57 : 29.88	−28 : 42 : 17.1	7.675599	5267.8518	0.2646	0.01221	15.492	17.101	39.99	1.00
OGLE-TR-1043	17 : 57 : 44.37	−27 : 58 : 28.5	2.196576	5378.07	0.091	0.0031	15.359	17.073	7.24	0.98
OGLE-TR-1044	17 : 57 : 54.98	−27 : 48 : 40.8	5.1944381	5380.3002	0.1583	0.0417	13.836	14.852	21.54	1.00
OGLE-TR-1045	17 : 57 : 55.52	−29 : 13 : 04.2	2.1355658	5262.4665	0.1623	0.0302	14.730	15.750	26.05	1.00
OGLE-TR-1046	17 : 57 : 56.84	−27 : 36 : 50.5	10.619790	5381.1543	0.2896	0.01414	15.245	16.751	34.92	0.96
OGLE-TR-1047	17 : 58 : 06.08	−27 : 46 : 06.7	10.295061	5378.3788	0.2506	0.01349	15.476	16.759	33.56	1.00
OGLE-TR-1048	17 : 58 : 07.33	−29 : 27 : 32.2	5.2472019	5378.6899	0.1735	0.01730	15.431	16.736	32.92	1.00
OGLE-TR-1049	17 : 58 : 17.11	−27 : 34 : 26.1	19.15773	5384.334	0.737	0.00122	14.629	16.007	6.33	1.00
OGLE-TR-1050	17 : 58 : 27.67	−29 : 49 : 32.0	1.6114682	5377.8440	0.1208	0.0152	15.269	16.204	41.03	0.97
OGLE-TR-1051	17 : 58 : 31.55	−29 : 16 : 55.4	1.0213727	5376.673	0.465	0.001312	15.324	17.065	17.85	0.97
OGLE-TR-1052	17 : 58 : 33.17	−29 : 23 : 01.1	6.921614	5377.348	0.534	0.00169	14.876	16.149	12.62	0.96

continued on next page

Table 3
Continued

Name	RA (J2000)	DEC (J2000)	P_{orb} [d]	T_c [BJD _{TDB} – 2450000]	T_{14} [d]	δ	I [mag]	V [mag]	SNR	Pr(planet signal)
OGLE-TR-1053	17:58:34.08	-28:48:24.9	3.6519106	5273.7362	0.1135	0.0109	14.915	15.829	47.88	1.00
OGLE-TR-1054	17:58:39.75	-27:22:32.0	8.58268	5378.537	0.342	0.00272	15.066	16.220	6.25	0.98
OGLE-TR-1055	17:58:41.82	-29:11:27.7	2.104221	5503.963	0.236	0.00135	14.919	16.800	7.99	0.95
OGLE-TR-1056	17:58:55.74	-28:53:03.8	7.7213	5263.3	0.195	0.00181	14.913	16.686	7.03	0.94
OGLE-TR-1057	17:59:05.12	-28:29:51.9	5.854539	5378.9814	0.586	0.00491	15.245	17.114	18.57	1.00
OGLE-TR-1058	17:59:14.69	-27:44:55.6	17.41082	5382.036	0.403	0.00217	14.806	16.222	8.02	0.94
OGLE-TR-1059	17:59:24.87	-28:01:37.4	7.208224	5377.8502	0.2321	0.00646	15.412	16.726	19.09	0.97
OGLE-TR-1060	17:59:27.20	-28:00:26.8	12.831750	5386.0147	0.2709	0.01508	15.307	16.677	34.86	1.00
OGLE-TR-1061	17:59:30.54	-27:23:20.3	2.6528610	5376.6303	0.1696	0.00915	14.119	14.767	55.65	1.00
OGLE-TR-1062	17:59:44.10	-28:05:53.7	16.52749	5383.916	0.327	0.00445	15.152	16.495	7.76	1.00
OGLE-TR-1063	17:59:51.37	-29:17:22.5	3.5835181	5261.3897	0.1596	0.01070	14.703	15.560	51.49	1.00
OGLE-TR-1064	18:00:00.26	-29:15:02.6	0.6700153	5286.4298	0.0945	0.00320	15.472	16.582	20.52	0.99
OGLE-TR-1065	18:00:17.82	-28:49:53.7	4.967119	5380.6973	0.194	0.00310	15.463	17.413	11.33	1.00
OGLE-TR-1066	18:00:24.34	-28:20:56.8	10.03302	5386.199	0.588	0.00219	15.257	16.412	11.24	0.84
OGLE-TR-1067	18:01:02.46	-29:09:54.7	2.573161	5376.738	0.325	0.00217	14.744	16.651	23.79	0.94
OGLE-TR-1068	18:01:11.74	-28:53:43.1	0.68587341	5376.9436	0.0858	0.00619	12.800	13.359	41.69	1.00
OGLE-TR-1069	18:01:16.03	-28:25:46.1	10.605366	5383.6787	0.5106	0.01568	15.339	16.611	54.25	1.00
OGLE-TR-1070	18:01:17.40	-28:30:28.0	1.7293835	5380.2336	0.1135	0.01428	15.400	16.324	34.25	0.81
OGLE-TR-1071	18:01:17.69	-28:48:23.4	4.26703	5383.137	0.458	0.0049	15.424	17.366	15.87	1.00
OGLE-TR-1072	18:01:20.90	-28:26:24.4	1.6133903	5377.4958	0.0986	0.00808	15.112	16.169	33.32	1.00
OGLE-TR-1073	18:01:28.64	-28:25:28.0	6.92344	5380.819	0.400	0.00130	15.283	17.176	6.60	1.00
OGLE-TR-1074	18:01:46.42	-28:00:52.9	0.7182068	5376.8768	0.0807	0.00344	15.167	16.364	24.77	0.92
OGLE-TR-1075	18:01:47.87	-28:01:19.6	30.55566	5390.5423	0.441	0.01590	15.297	16.490	39.16	1.00
OGLE-TR-1076	18:01:59.91	-28:46:32.9	5.785527	5380.2351	0.2844	0.01468	15.057	16.128	25.86	1.00
OGLE-TR-1077	18:02:01.98	-28:43:15.8	14.40827	5381.544	0.255	0.00397	14.606	15.541	6.52	0.99
OGLE-TR-1078	18:02:16.54	-29:05:43.6	4.3297076	5377.6280	0.2245	0.00740	14.700	15.665	45.05	1.00
OGLE-TR-1079	18:02:44.77	-28:48:25.6	13.45047	5381.447	0.554	0.00294	15.351	17.201	7.58	1.00

continued on next page

Table 3
Continued

Name	RA (J2000)	DEC (J2000)	P_{orb} [d]	T_c [BJD _{TDB} − 2450000]	T_{14} [d]	δ	I [mag]	V [mag]	SNR	Pr(planet signal)
OGLE-TR-1080	18 : 02 : 50.21	−28 : 21 : 44.1	4.7576944	5377.9397	0.2339	0.00446	14.871	16.122	25.76	1.00
OGLE-TR-1081	18 : 03 : 14.00	−28 : 27 : 14.8	6.406942	5377.5162	0.1741	0.00608	14.978	15.934	23.62	1.00
OGLE-TR-1082	18 : 03 : 15.26	−28 : 45 : 00.7	3.403645	5379.0038	0.379	0.00377	15.398	17.377	18.94	1.00
OGLE-TR-1083	18 : 03 : 15.36	−28 : 24 : 25.6	5.410081	5380.6355	0.1406	0.01005	15.057	16.084	20.41	1.00
OGLE-TR-1084	18 : 03 : 18.58	−28 : 24 : 45.1	39.79726	5402.3122	0.2763	0.01558	14.141	14.969	39.18	0.94
OGLE-TR-1085	18 : 03 : 21.39	−28 : 12 : 40.2	3.636724	5377.8549	0.129	0.00316	15.362	17.017	12.74	1.00
OGLE-TR-1086	18 : 03 : 39.15	−28 : 47 : 04.6	6.703196	5383.100	0.237	0.00510	15.324	16.785	17.18	0.94
OGLE-TR-1087	18 : 03 : 46.16	−28 : 07 : 56.2	4.243165	5378.3633	0.206	0.00654	15.148	16.438	30.74	1.00
OGLE-TR-1088	18 : 03 : 47.49	−28 : 05 : 03.0	5.0748842	5378.05549	0.1469	0.01584	14.438	15.373	66.06	1.00
OGLE-TR-1089	18 : 04 : 07.51	−28 : 41 : 30.5	51.09021	5384.643	0.346	0.0186	14.961	16.088	15.94	1.00
OGLE-TR-1090	18 : 04 : 14.72	−28 : 20 : 22.9	6.555184	5376.6412	0.2352	0.00525	14.240	14.918	18.22	1.00
OGLE-TR-1091	18 : 04 : 18.26	−28 : 24 : 30.5	55.74533	5427.429	0.429	0.0129	15.249	17.054	21.54	0.99
OGLE-TR-1092	18 : 04 : 23.84	−28 : 48 : 50.7	3.660176	5380.164	0.212	0.00188	15.294	16.873	7.65	1.00
OGLE-TR-1093	18 : 04 : 46.65	−28 : 57 : 20.9	1.4751354	5377.1974	0.134	0.0113	14.756	16.523	80.19	0.98
OGLE-TR-1094	18 : 04 : 49.42	−28 : 00 : 44.0	13.20038	5388.402	0.312	0.0102	15.497	17.402	9.66	1.00
OGLE-TR-1095	18 : 04 : 53.49	−28 : 13 : 33.0	0.7848204	5377.2801	0.0864	0.00282	15.239	17.210	15.83	0.90
OGLE-TR-1096	18 : 05 : 07.41	−28 : 15 : 56.6	3.437753	5377.2231	0.446	0.00514	15.446	17.249	27.43	1.00
OGLE-TR-1097	18 : 05 : 15.35	−28 : 08 : 47.3	10.756626	5385.3247	0.1199	0.01424	15.128	16.745	29.74	0.90
OGLE-TR-1098	18 : 05 : 29.39	−28 : 15 : 28.8	5.880841	5379.1189	0.1454	0.0203	15.372	16.404	40.22	0.93
OGLE-TR-1099	18 : 05 : 36.98	−28 : 28 : 27.6	10.46173	5376.945	0.630	0.00279	15.369	17.213	14.37	1.00

Table 4
Selected physical parameters of systems with planetary candidates.

Name	M_*	R_*	logg	T_{eff}	[Fe/H]	d	a	i	T_{eq}	R_P
	$[M_\odot]$	$[R_\odot]$	[cgs]	[K]	[dex]	[pc]	[AU]	[deg]	[K]	$[R_J]$
OGLE-TR-1001	$2.44^{+0.42}_{-0.36}$	$1.57^{+0.23}_{-0.14}$	$4.42^{+0.13}_{-0.15}$	14400^{+2500}_{-3800}	$-1.5^{+1.5}_{-1.6}$	1810^{+91}_{-79}	$0.0437^{+0.0023}_{-0.0024}$	$84.2^{+2.1}_{-2.3}$	4190^{+480}_{-860}	$1.39^{+0.22}_{-0.14}$
OGLE-TR-1002	$1.27^{+0.12}_{-0.14}$	$1.429^{+0.086}_{-0.099}$	$4.232^{+0.062}_{-0.059}$	6030^{+310}_{-280}	$0.38^{+0.11}_{-0.18}$	1660^{+130}_{-120}	$0.1184^{+0.0036}_{-0.0044}$	$87.28^{+0.26}_{-0.22}$	1007^{+51}_{-46}	$1.66^{+0.12}_{-0.15}$
OGLE-TR-1003	$0.927^{+0.130}_{-0.090}$	$1.021^{+0.098}_{-0.075}$	$4.393^{+0.051}_{-0.067}$	5770^{+310}_{-250}	$-0.11^{+0.23}_{-0.40}$	1088^{+120}_{-93}	$0.0377^{+0.0017}_{-0.0013}$	$88.2^{+1.2}_{-1.7}$	1452^{+96}_{-78}	$0.529^{+0.057}_{-0.042}$
OGLE-TR-1004	$1.93^{+0.14}_{-0.14}$	$1.96^{+0.19}_{-0.18}$	$4.142^{+0.077}_{-0.079}$	7780^{+400}_{-400}	$0.31^{+0.12}_{-0.19}$	1690^{+140}_{-130}	$0.1166^{+0.0029}_{-0.0033}$	$86.64^{+0.46}_{-0.51}$	1536^{+76}_{-73}	$1.52^{+0.16}_{-0.16}$
OGLE-TR-1005	$0.965^{+0.330}_{-0.075}$	$1.763^{+0.210}_{-0.090}$	$3.949^{+0.052}_{-0.062}$	7800^{+830}_{-470}	$-3.99^{+1.20}_{-0.31}$	2210^{+260}_{-130}	$0.0533^{+0.0055}_{-0.0014}$	$87.9^{+1.5}_{-1.8}$	2160^{+230}_{-120}	$1.389^{+0.180}_{-0.078}$
OGLE-TR-1006	$1.74^{+0.14}_{-0.17}$	$2.19^{+0.20}_{-0.15}$	$4.003^{+0.044}_{-0.086}$	5310^{+300}_{-310}	$0.30^{+0.21}_{-0.26}$	1520^{+120}_{-97}	$0.03521^{+0.00090}_{-0.00110}$	$75.1^{+1.1}_{-2.0}$	2022^{+100}_{-84}	$1.131^{+0.150}_{-0.088}$
OGLE-TR-1007	$1.65^{+0.21}_{-0.12}$	$2.95^{+0.24}_{-0.23}$	$3.726^{+0.053}_{-0.053}$	6800^{+580}_{-520}	$-3.32^{+1.50}_{-0.49}$	1690^{+170}_{-160}	$0.0569^{+0.0020}_{-0.0015}$	$78.22^{+0.96}_{-1.00}$	2350^{+210}_{-180}	$2.98^{+0.29}_{-0.27}$
OGLE-TR-1008	$0.98^{+0.29}_{-0.35}$	$2.10^{+0.19}_{-0.16}$	$3.78^{+0.15}_{-0.20}$	5130^{+430}_{-390}	$-2.3^{+2.0}_{-1.4}$	1770^{+130}_{-120}	$0.312^{+0.028}_{-0.041}$	$88.87^{+0.49}_{-0.44}$	652^{+51}_{-56}	$1.170^{+0.110}_{-0.087}$
OGLE-TR-1009	$4.19^{+0.56}_{-0.52}$	$2.185^{+0.098}_{-0.094}$	$4.382^{+0.027}_{-0.030}$	21600^{+1800}_{-2100}	$-3.13^{+1.00}_{-0.57}$	3160^{+300}_{-280}	$0.302^{+0.013}_{-0.013}$	$89.80^{+0.14}_{-0.21}$	2800^{+230}_{-260}	$2.218^{+0.099}_{-0.096}$
OGLE-TR-1010	$0.826^{+0.039}_{-0.039}$	$1.711^{+0.140}_{-0.095}$	$3.888^{+0.056}_{-0.072}$	6900^{+260}_{-270}	$-4.437^{+0.130}_{-0.076}$	1695^{+96}_{-80}	$0.03116^{+0.00048}_{-0.00050}$	$83.9^{+3.0}_{-2.8}$	2470^{+88}_{-81}	$1.390^{+0.140}_{-0.092}$
OGLE-TR-1011	$1.56^{+0.22}_{-0.17}$	$1.94^{+0.42}_{-0.27}$	$4.070^{+0.086}_{-0.160}$	5150^{+380}_{-300}	$0.31^{+0.20}_{-0.23}$	1870^{+310}_{-210}	$0.1525^{+0.0080}_{-0.0075}$	$88.6^{+1.0}_{-1.3}$	896^{+62}_{-51}	$1.52^{+0.42}_{-0.25}$
OGLE-TR-1012	$1.88^{+0.19}_{-0.25}$	$1.78^{+0.15}_{-0.12}$	$4.205^{+0.056}_{-0.088}$	8170^{+450}_{-400}	$0.10^{+0.25}_{-0.49}$	2490^{+260}_{-220}	$0.0569^{+0.0018}_{-0.0025}$	$86.4^{+1.8}_{-1.6}$	2220^{+140}_{-110}	$1.088^{+0.099}_{-0.075}$
OGLE-TR-1013	$2.00^{+0.60}_{-0.55}$	$1.47^{+0.13}_{-0.12}$	$4.40^{+0.13}_{-0.15}$	12100^{+3200}_{-2100}	$-1.59^{+0.93}_{-1.50}$	2670^{+350}_{-260}	$0.206^{+0.019}_{-0.021}$	$89.05^{+0.56}_{-0.48}$	1570^{+310}_{-220}	$1.049^{+0.085}_{-0.075}$
OGLE-TR-1014	$0.93^{+0.21}_{-0.11}$	$1.93^{+0.15}_{-0.14}$	$3.842^{+0.110}_{-0.086}$	6020^{+640}_{-560}	$-0.76^{+0.47}_{-1.20}$	1100^{+67}_{-60}	$0.1023^{+0.0068}_{-0.0040}$	$88.1^{+1.3}_{-1.2}$	1252^{+110}_{-91}	$0.944^{+0.070}_{-0.067}$
OGLE-TR-1015	$0.916^{+0.160}_{-0.094}$	$2.26^{+0.28}_{-0.21}$	$3.696^{+0.094}_{-0.100}$	5530^{+520}_{-370}	$-0.69^{+0.38}_{-0.87}$	2690^{+350}_{-270}	$0.1250^{+0.0067}_{-0.0044}$	$88.5^{+1.0}_{-1.2}$	1143^{+100}_{-81}	$1.071^{+0.098}_{-0.076}$

continued on next page

Table 4

Continued

Name	M_*	R_*	logg	T_{eff}	[Fe/H]	d	a	i	T_{eq}	R_P
	$[M_\odot]$	$[R_\odot]$	[cgs]	[K]	[dex]	[pc]	[AU]	[deg]	[K]	$[R_J]$
OGLE-TR-1016	$1.01^{+0.42}_{-0.18}$	$2.32^{+0.29}_{-0.31}$	$3.72^{+0.21}_{-0.14}$	5620^{+650}_{-510}	$-0.29^{+0.42}_{-1.20}$	2680^{+320}_{-290}	$0.0495^{+0.0058}_{-0.0029}$	$79.9^{+2.0}_{-1.9}$	1830^{+190}_{-130}	$0.983^{+0.088}_{-0.084}$
OGLE-TR-1017	$1.90^{+0.91}_{-0.50}$	$1.28^{+0.44}_{-0.16}$	$4.49^{+0.23}_{-0.29}$	12700^{+5200}_{-5100}	$-2.6^{+2.7}_{-1.1}$	2860^{+630}_{-570}	$0.100^{+0.014}_{-0.010}$	$87.9^{+1.5}_{-1.9}$	2200^{+650}_{-690}	$1.34^{+0.62}_{-0.18}$
OGLE-TR-1018	$1.24^{+0.25}_{-0.28}$	$1.57^{+0.14}_{-0.12}$	$4.134^{+0.087}_{-0.120}$	6360^{+820}_{-630}	$0.04^{+0.32}_{-1.20}$	1890^{+240}_{-210}	$0.0517^{+0.0031}_{-0.0041}$	$86.2^{+1.9}_{-1.7}$	1690^{+240}_{-160}	$1.021^{+0.093}_{-0.080}$
OGLE-TR-1019	$0.820^{+0.078}_{-0.048}$	$1.385^{+0.079}_{-0.069}$	$4.076^{+0.049}_{-0.051}$	6970^{+410}_{-330}	$-4.28^{+1.20}_{-0.24}$	1219^{+89}_{-80}	$0.1485^{+0.0045}_{-0.0029}$	$89.65^{+0.24}_{-0.35}$	1026^{+58}_{-51}	$1.975^{+0.100}_{-0.092}$
OGLE-TR-1020	$0.57^{+0.17}_{-0.28}$	$0.865^{+0.055}_{-0.041}$	$4.29^{+0.12}_{-0.25}$	3710^{+190}_{-110}	$0.16^{+0.24}_{-1.60}$	411^{+29}_{-26}	$0.182^{+0.017}_{-0.038}$	$89.858^{+0.098}_{-0.330}$	403^{+34}_{-30}	$1.206^{+0.140}_{-0.085}$
OGLE-TR-1021	$1.504^{+0.100}_{-0.085}$	$1.459^{+0.062}_{-0.059}$	$4.288^{+0.029}_{-0.029}$	6990^{+360}_{-250}	$0.17^{+0.18}_{-0.14}$	1586^{+85}_{-77}	$0.3053^{+0.0067}_{-0.0058}$	$89.199^{+0.074}_{-0.072}$	737^{+36}_{-28}	$2.20^{+0.11}_{-0.10}$
OGLE-TR-1022	$0.871^{+0.064}_{-0.063}$	$2.59^{+0.69}_{-0.32}$	$3.56^{+0.11}_{-0.23}$	6490^{+450}_{-790}	$-4.16^{+0.96}_{-0.17}$	1910^{+210}_{-140}	$0.0778^{+0.0025}_{-0.0024}$	$84.1^{+1.7}_{-2.9}$	1801^{+69}_{-74}	$1.45^{+0.47}_{-0.22}$
OGLE-TR-1023	$1.331^{+0.091}_{-0.110}$	$1.386^{+0.071}_{-0.073}$	$4.279^{+0.040}_{-0.046}$	6290^{+250}_{-240}	$0.34^{+0.14}_{-0.21}$	1481^{+93}_{-87}	$0.0757^{+0.0017}_{-0.0021}$	$85.92^{+0.29}_{-0.28}$	1296^{+56}_{-51}	$1.71^{+0.11}_{-0.12}$
OGLE-TR-1024	$1.44^{+0.27}_{-1.00}$	$2.03^{+0.17}_{-0.15}$	$3.96^{+0.10}_{-0.48}$	5190^{+430}_{-430}	$-0.09^{+0.42}_{-3.20}$	1630^{+180}_{-160}	$0.0283^{+0.0016}_{-0.0089}$	$77.0^{+4.6}_{-11.0}$	2230^{+210}_{-160}	$1.029^{+0.086}_{-0.081}$
OGLE-TR-1025	$0.42^{+1.10}_{-0.14}$	$2.85^{+0.23}_{-0.21}$	$3.16^{+0.50}_{-0.20}$	4880^{+260}_{-240}	$-3.34^{+3.30}_{-0.48}$	1980^{+190}_{-150}	$0.0550^{+0.0280}_{-0.0064}$	$79.2^{+5.8}_{-2.8}$	1670^{+110}_{-180}	$1.030^{+0.080}_{-0.074}$
OGLE-TR-1026	$0.857^{+0.140}_{-0.067}$	$2.73^{+0.32}_{-0.28}$	$3.503^{+0.100}_{-0.082}$	5760^{+480}_{-430}	$-1.76^{+0.94}_{-1.20}$	1710^{+240}_{-180}	$0.0484^{+0.0026}_{-0.0015}$	$87.4^{+1.8}_{-3.0}$	2100^{+170}_{-170}	$1.196^{+0.140}_{-0.090}$
OGLE-TR-1027	$2.06^{+0.47}_{-0.51}$	$2.95^{+1.10}_{-0.39}$	$3.80^{+0.11}_{-0.28}$	5320^{+370}_{-290}	$0.26^{+0.23}_{-0.35}$	2570^{+780}_{-340}	$0.0477^{+0.0042}_{-0.0037}$	$75.2^{+2.5}_{-7.7}$	2090^{+240}_{-170}	$1.21^{+1.20}_{-0.15}$
OGLE-TR-1028	$1.11^{+0.19}_{-0.14}$	$2.06^{+0.23}_{-0.16}$	$3.854^{+0.085}_{-0.095}$	5290^{+510}_{-330}	$0.22^{+0.23}_{-0.26}$	1130^{+130}_{-99}	$0.01676^{+0.00090}_{-0.00074}$	$60.3^{+4.1}_{-5.2}$	2830^{+240}_{-160}	$1.40^{+0.22}_{-0.14}$
OGLE-TR-1029	$1.025^{+0.075}_{-0.085}$	$0.995^{+0.050}_{-0.039}$	$4.453^{+0.029}_{-0.043}$	5650^{+210}_{-200}	$0.23^{+0.19}_{-0.19}$	1183^{+78}_{-70}	$0.03711^{+0.00088}_{-0.00100}$	$87.9^{+1.2}_{-1.1}$	1414^{+62}_{-55}	$1.067^{+0.065}_{-0.047}$
OGLE-TR-1030	$1.40^{+0.11}_{-0.12}$	$1.556^{+0.160}_{-0.097}$	$4.204^{+0.058}_{-0.098}$	6280^{+330}_{-330}	$0.37^{+0.11}_{-0.17}$	1536^{+120}_{-99}	$0.1517^{+0.0039}_{-0.0045}$	$88.88^{+0.62}_{-0.65}$	974^{+49}_{-41}	$1.381^{+0.190}_{-0.099}$
OGLE-TR-1031	$1.15^{+0.22}_{-0.17}$	$1.96^{+0.17}_{-0.15}$	$3.919^{+0.095}_{-0.110}$	5490^{+330}_{-420}	$0.18^{+0.23}_{-0.24}$	1410^{+130}_{-110}	$0.0374^{+0.0021}_{-0.0018}$	$85.5^{+3.0}_{-3.4}$	1901^{+92}_{-84}	$1.009^{+0.073}_{-0.068}$
OGLE-TR-1032	$1.417^{+0.084}_{-0.051}$	$1.699^{+0.050}_{-0.040}$	$4.131^{+0.014}_{-0.015}$	5860^{+290}_{-280}	$0.45^{+0.11}_{-0.21}$	1598^{+83}_{-74}	$0.1287^{+0.0025}_{-0.0016}$	$89.65^{+0.25}_{-0.36}$	1026^{+50}_{-49}	$2.232^{+0.067}_{-0.050}$

continued on next page

Table 4

Continued

Name	M_*	R_*	logg	T_{eff}	[Fe/H]	d	a	i	T_{eq}	R_{P}
	$[M_{\odot}]$	$[R_{\odot}]$	[cgs]	[K]	[dex]	[pc]	[AU]	[deg]	[K]	$[R_{\text{J}}]$
OGLE-TR-1033	$0.883^{+0.120}_{-0.083}$	$1.725^{+0.150}_{-0.082}$	$3.916^{+0.041}_{-0.062}$	7090^{+550}_{-420}	$-3.57^{+1.10}_{-0.42}$	1880^{+160}_{-130}	$0.1286^{+0.0055}_{-0.0041}$	$89.18^{+0.58}_{-0.82}$	1258^{+92}_{-73}	$1.381^{+0.130}_{-0.072}$
OGLE-TR-1034	$0.782^{+0.032}_{-0.022}$	$1.434^{+0.061}_{-0.061}$	$4.022^{+0.041}_{-0.037}$	6530^{+210}_{-200}	$-4.480^{+0.080}_{-0.059}$	1409^{+75}_{-72}	$0.05554^{+0.00075}_{-0.00052}$	$85.05^{+0.44}_{-0.41}$	1598^{+54}_{-53}	$2.02^{+0.11}_{-0.10}$
OGLE-TR-1035	$1.633^{+0.096}_{-0.092}$	$1.601^{+0.070}_{-0.067}$	$4.244^{+0.037}_{-0.042}$	7230^{+330}_{-290}	$0.15^{+0.16}_{-0.13}$	1262^{+42}_{-39}	$0.3344^{+0.0064}_{-0.0064}$	$88.950^{+0.067}_{-0.068}$	763^{+29}_{-25}	$1.73^{+0.11}_{-0.11}$
OGLE-TR-1036	$0.794^{+0.083}_{-0.034}$	$1.329^{+0.050}_{-0.043}$	$4.099^{+0.028}_{-0.025}$	6690^{+320}_{-380}	$-3.51^{+2.10}_{-0.86}$	1096^{+87}_{-78}	$0.01739^{+0.00059}_{-0.00025}$	$71.70^{+0.71}_{-0.75}$	2810^{+140}_{-170}	$1.668^{+0.110}_{-0.091}$
OGLE-TR-1037	$1.42^{+0.32}_{-0.59}$	$2.56^{+0.26}_{-0.22}$	$3.78^{+0.13}_{-0.27}$	6090^{+440}_{-750}	$0.00^{+0.31}_{-2.30}$	2280^{+200}_{-170}	$0.0778^{+0.0053}_{-0.0120}$	$83.3^{+1.6}_{-2.3}$	1690^{+120}_{-110}	$1.001^{+0.085}_{-0.080}$
OGLE-TR-1038	$0.271^{+0.110}_{-0.073}$	$2.66^{+0.19}_{-0.18}$	$3.02^{+0.17}_{-0.15}$	4630^{+230}_{-220}	$-3.51^{+0.68}_{-0.35}$	1187^{+41}_{-40}	$0.0352^{+0.0031}_{-0.0028}$	$84.5^{+3.9}_{-5.0}$	1936^{+100}_{-80}	$1.79^{+0.22}_{-0.39}$
OGLE-TR-1039	$1.63^{+0.18}_{-0.24}$	$2.12^{+0.21}_{-0.15}$	$3.992^{+0.084}_{-0.130}$	6700^{+480}_{-430}	$0.08^{+0.22}_{-0.21}$	2320^{+220}_{-170}	$0.1017^{+0.0037}_{-0.0052}$	$85.53^{+0.62}_{-0.91}$	1485^{+91}_{-78}	$1.167^{+0.150}_{-0.096}$
OGLE-TR-1040	$1.00^{+0.25}_{-0.16}$	$0.993^{+0.079}_{-0.068}$	$4.450^{+0.100}_{-0.098}$	7370^{+1700}_{-810}	$-2.8^{+1.6}_{-1.2}$	2010^{+350}_{-270}	$0.1438^{+0.0110}_{-0.0081}$	$89.08^{+0.40}_{-0.33}$	940^{+180}_{-110}	$1.058^{+0.093}_{-0.078}$
OGLE-TR-1041	$1.06^{+0.21}_{-0.14}$	$1.248^{+0.069}_{-0.061}$	$4.279^{+0.035}_{-0.043}$	7190^{+790}_{-1100}	$-1.4^{+1.6}_{-2.1}$	1370^{+82}_{-76}	$0.0423^{+0.0025}_{-0.0018}$	$88.73^{+0.88}_{-1.30}$	1880^{+200}_{-290}	$1.140^{+0.060}_{-0.054}$
OGLE-TR-1042	$0.871^{+0.150}_{-0.092}$	$1.546^{+0.086}_{-0.071}$	$4.006^{+0.025}_{-0.026}$	5980^{+420}_{-460}	$-0.80^{+0.80}_{-1.90}$	1390^{+120}_{-100}	$0.0727^{+0.0039}_{-0.0027}$	$89.33^{+0.47}_{-0.73}$	1327^{+94}_{-100}	$1.662^{+0.087}_{-0.073}$
OGLE-TR-1043	$1.26^{+0.18}_{-0.17}$	$1.86^{+0.43}_{-0.26}$	$3.99^{+0.14}_{-0.16}$	5750^{+350}_{-380}	$0.24^{+0.17}_{-0.22}$	1670^{+320}_{-230}	$0.0361^{+0.0017}_{-0.0018}$	$78.2^{+2.1}_{-1.7}$	1990^{+160}_{-130}	$1.003^{+0.093}_{-0.084}$
OGLE-TR-1044	$1.010^{+0.070}_{-0.069}$	$1.014^{+0.030}_{-0.029}$	$4.431^{+0.030}_{-0.033}$	5580^{+130}_{-120}	$0.34^{+0.14}_{-0.16}$	804^{+22}_{-21}	$0.0589^{+0.0013}_{-0.0014}$	$89.47^{+0.37}_{-0.53}$	1117^{+23}_{-23}	$2.015^{+0.066}_{-0.064}$
OGLE-TR-1045	$0.797^{+0.074}_{-0.038}$	$1.317^{+0.052}_{-0.041}$	$4.106^{+0.025}_{-0.026}$	7000^{+370}_{-300}	$-4.18^{+0.99}_{-0.27}$	1810^{+190}_{-190}	$0.03010^{+0.00090}_{-0.00048}$	$88.97^{+0.75}_{-1.10}$	2227^{+120}_{-91}	$2.228^{+0.082}_{-0.070}$
OGLE-TR-1046	$0.993^{+0.097}_{-0.079}$	$1.570^{+0.065}_{-0.064}$	$4.044^{+0.026}_{-0.029}$	5560^{+380}_{-220}	$0.05^{+0.23}_{-0.25}$	1391^{+99}_{-84}	$0.0943^{+0.0030}_{-0.0026}$	$89.47^{+0.37}_{-0.56}$	1094^{+74}_{-43}	$1.813^{+0.078}_{-0.071}$
OGLE-TR-1047	$0.90^{+0.12}_{-0.18}$	$1.347^{+0.081}_{-0.085}$	$4.134^{+0.036}_{-0.064}$	5530^{+270}_{-250}	$-3.45^{+0.84}_{-0.38}$	1720^{+140}_{-140}	$0.0896^{+0.0038}_{-0.0064}$	$89.17^{+0.58}_{-0.82}$	1039^{+52}_{-48}	$1.519^{+0.100}_{-0.099}$
OGLE-TR-1048	$0.85^{+0.21}_{-0.31}$	$1.15^{+0.16}_{-0.15}$	$4.230^{+0.062}_{-0.100}$	5400^{+1100}_{-430}	$-2.5^{+1.8}_{-1.1}$	1530^{+240}_{-190}	$0.0573^{+0.0054}_{-0.0084}$	$88.78^{+0.87}_{-1.40}$	1186^{+220}_{-97}	$1.47^{+0.22}_{-0.20}$
OGLE-TR-1049	$0.71^{+0.47}_{-0.19}$	$3.40^{+0.33}_{-0.25}$	$3.22^{+0.22}_{-0.13}$	5290^{+280}_{-330}	$-2.63^{+1.20}_{-0.85}$	2440^{+230}_{-180}	$0.128^{+0.022}_{-0.012}$	$88.1^{+1.3}_{-1.9}$	1306^{+77}_{-75}	$1.144^{+0.120}_{-0.083}$

continued on next page

Table 4

Continued

Name	M_*	R_*	logg	T_{eff}	[Fe/H]	d	a	i	T_{eq}	R_P
	$[M_\odot]$	$[R_\odot]$	[cgs]	[K]	[dex]	[pc]	[AU]	[deg]	[K]	$[R_J]$
OGLE-TR-1050	$0.122^{+0.061}_{-0.017}$	$0.953^{+0.069}_{-0.052}$	$3.579^{+0.130}_{-0.059}$	4740^{+240}_{-200}	$-3.01^{+0.81}_{-0.65}$	962^{+100}_{-89}	$0.01415^{+0.00170}_{-0.00089}$	$74.5^{+2.0}_{-1.5}$	1860^{+110}_{-110}	$1.152^{+0.093}_{-0.080}$
OGLE-TR-1051	$0.946^{+0.120}_{-0.073}$	$4.00^{+0.21}_{-0.15}$	$3.210^{+0.031}_{-0.018}$	4770^{+140}_{-150}	$-0.20^{+0.23}_{-0.38}$	2880^{+220}_{-180}	$0.01956^{+0.00098}_{-0.00055}$	$78.8^{+7.8}_{-12.0}$	3280^{+100}_{-110}	$1.407^{+0.100}_{-0.069}$
OGLE-TR-1052	$1.01^{+0.57}_{-0.21}$	$6.0^{+1.6}_{-1.9}$	$2.88^{+0.47}_{-0.20}$	5360^{+320}_{-280}	$-2.5^{+2.3}_{-1.1}$	4900^{+1600}_{-1300}	$0.0765^{+0.0084}_{-0.0051}$	$72.0^{+13.0}_{-6.2}$	2260^{+290}_{-400}	$2.44^{+0.76}_{-0.99}$
OGLE-TR-1053	$1.11^{+0.41}_{-0.23}$	$1.53^{+0.27}_{-0.24}$	$4.128^{+0.110}_{-0.098}$	7250^{+650}_{-530}	$-1.10^{+0.86}_{-2.20}$	2030^{+360}_{-260}	$0.0493^{+0.0057}_{-0.0040}$	$82.8^{+1.2}_{-1.1}$	1930^{+170}_{-130}	$1.57^{+0.47}_{-0.31}$
OGLE-TR-1054	$1.55^{+0.34}_{-0.27}$	$2.51^{+0.49}_{-0.30}$	$3.80^{+0.16}_{-0.15}$	6060^{+940}_{-570}	$-1.5^{+1.7}_{-1.7}$	2670^{+360}_{-270}	$0.0961^{+0.0065}_{-0.0061}$	$88.2^{+1.3}_{-2.4}$	1540^{+140}_{-110}	$1.22^{+0.41}_{-0.12}$
OGLE-TR-1055	$0.97^{+0.21}_{-0.11}$	$3.00^{+0.33}_{-0.25}$	$3.477^{+0.093}_{-0.100}$	5090^{+230}_{-190}	$-0.46^{+0.23}_{-0.48}$	1830^{+260}_{-200}	$0.0323^{+0.0021}_{-0.0013}$	$72.5^{+4.0}_{-4.3}$	2370^{+180}_{-130}	$1.067^{+0.110}_{-0.089}$
OGLE-TR-1056	$1.071^{+0.110}_{-0.066}$	$2.55^{+0.48}_{-0.38}$	$3.66^{+0.15}_{-0.13}$	4690^{+160}_{-150}	$0.41^{+0.13}_{-0.20}$	1690^{+310}_{-220}	$0.0791^{+0.0024}_{-0.0018}$	$82.3^{+1.2}_{-1.3}$	1281^{+110}_{-99}	$1.048^{+0.085}_{-0.078}$
OGLE-TR-1057	$0.782^{+0.029}_{-0.014}$	$3.67^{+0.10}_{-0.10}$	$3.206^{+0.024}_{-0.023}$	5590^{+220}_{-240}	$-2.71^{+1.00}_{-0.91}$	5400^{+1400}_{-1300}	$0.05857^{+0.00071}_{-0.00034}$	$88.86^{+0.80}_{-1.20}$	2130^{+89}_{-95}	$2.498^{+0.084}_{-0.084}$
OGLE-TR-1058	$1.82^{+0.16}_{-0.17}$	$2.62^{+0.36}_{-0.23}$	$3.854^{+0.082}_{-0.110}$	6640^{+450}_{-360}	$0.26^{+0.14}_{-0.20}$	2460^{+280}_{-200}	$0.1615^{+0.0052}_{-0.0051}$	$88.5^{+1.0}_{-1.1}$	1299^{+81}_{-69}	$1.171^{+0.170}_{-0.089}$
OGLE-TR-1059	$1.02^{+0.31}_{-0.19}$	$1.48^{+0.13}_{-0.11}$	$4.11^{+0.12}_{-0.10}$	6820^{+850}_{-610}	$-1.4^{+1.4}_{-2.0}$	1590^{+130}_{-110}	$0.0741^{+0.0068}_{-0.0049}$	$88.3^{+1.1}_{-1.1}$	$1490.00^{+0.37}_{-0.19}$	$1.152^{+0.096}_{-0.077}$
OGLE-TR-1060	$1.116^{+0.200}_{-0.089}$	$1.532^{+0.096}_{-0.093}$	$4.127^{+0.070}_{-0.073}$	6190^{+560}_{-490}	$-3.29^{+3.50}_{-0.53}$	1810^{+140}_{-130}	$0.1113^{+0.0064}_{-0.0030}$	$88.52^{+0.85}_{-0.64}$	1100^{+91}_{-64}	$1.83^{+0.14}_{-0.12}$
OGLE-TR-1061	$1.79^{+0.24}_{-0.58}$	$1.805^{+0.086}_{-0.170}$	$4.173^{+0.031}_{-0.069}$	8510^{+1100}_{-520}	$-0.15^{+0.44}_{-2.90}$	2090^{+140}_{-150}	$0.0455^{+0.0020}_{-0.0056}$	$88.3^{+1.2}_{-1.8}$	2600^{+340}_{-160}	$1.678^{+0.081}_{-0.160}$
OGLE-TR-1062	$1.01^{+0.14}_{-0.16}$	$1.70^{+0.16}_{-0.16}$	$3.981^{+0.110}_{-0.096}$	6870^{+650}_{-900}	$-1.6^{+1.5}_{-2.2}$	1960^{+550}_{-350}	$0.1289^{+0.0052}_{-0.0078}$	$89.07^{+0.64}_{-0.59}$	1220^{+140}_{-180}	$1.102^{+0.061}_{-0.068}$
OGLE-TR-1063	$1.12^{+0.40}_{-0.13}$	$1.382^{+0.120}_{-0.082}$	$4.233^{+0.059}_{-0.076}$	8290^{+440}_{-490}	$-1.9^{+1.4}_{-1.6}$	1527^{+89}_{-77}	$0.0476^{+0.0051}_{-0.0019}$	$87.6^{+1.5}_{-1.5}$	2137^{+99}_{-110}	$1.392^{+0.130}_{-0.090}$
OGLE-TR-1064	$1.09^{+0.27}_{-0.50}$	$1.87^{+0.14}_{-0.13}$	$3.92^{+0.11}_{-0.24}$	5240^{+430}_{-310}	$-1.22^{+0.76}_{-0.96}$	2300^{+220}_{-200}	$0.0156^{+0.0012}_{-0.0028}$	$61.9^{+5.7}_{-11.0}$	2850^{+200}_{-200}	$1.045^{+0.130}_{-0.097}$
OGLE-TR-1065	$0.93^{+0.36}_{-0.26}$	$1.87^{+0.12}_{-0.14}$	$3.83^{+0.19}_{-0.12}$	4270^{+240}_{-220}	$0.25^{+0.24}_{-0.38}$	1270^{+310}_{-140}	$0.0564^{+0.0064}_{-0.0056}$	$83.8^{+1.4}_{-1.3}$	1184^{+62}_{-52}	$1.024^{+0.058}_{-0.092}$
OGLE-TR-1066	$0.881^{+0.220}_{-0.088}$	$3.70^{+1.40}_{-0.77}$	$3.28^{+0.15}_{-0.25}$	5430^{+370}_{-400}	$-1.7^{+1.2}_{-1.6}$	4540^{+1600}_{-880}	$0.0917^{+0.0075}_{-0.0062}$	$86.8^{+2.4}_{-6.6}$	1670^{+210}_{-150}	$1.68^{+0.75}_{-0.39}$

continued on next page

Table 4
Continued

Name	M_*	R_*	logg	T_{eff}	[Fe/H]	d	a	i	T_{eq}	R_{P}
	$[M_{\odot}]$	$[R_{\odot}]$	[cgs]	[K]	[dex]	[pc]	[AU]	[deg]	[K]	$[R_J]$
OGLE-TR-1067	$1.25^{+0.24}_{-0.19}$	$5.52^{+0.61}_{-0.75}$	$3.051^{+0.140}_{-0.099}$	4620^{+140}_{-140}	$0.36^{+0.16}_{-0.20}$	2800^{+320}_{-360}	$0.0417^{+0.0023}_{-0.0018}$	$56.0^{+7.1}_{-5.1}$	2550^{+130}_{-160}	$2.51^{+0.44}_{-0.49}$
OGLE-TR-1068	$1.67^{+0.14}_{-0.15}$	$2.27^{+0.27}_{-0.43}$	$3.944^{+0.160}_{-0.089}$	6820^{+360}_{-310}	$0.09^{+0.19}_{-0.14}$	1430^{+180}_{-200}	$0.01856^{+0.00069}_{-0.00074}$	$58.6^{+7.2}_{-6.1}$	3600^{+180}_{-190}	$1.74^{+0.86}_{-0.44}$
OGLE-TR-1069	$0.7726^{+0.0190}_{-0.0089}$	$2.506^{+0.037}_{-0.034}$	$3.530^{+0.011}_{-0.011}$	5950^{+230}_{-260}	$-2.96^{+0.97}_{-0.83}$	3010^{+170}_{-160}	$0.08670^{+0.00071}_{-0.00033}$	$89.62^{+0.27}_{-0.42}$	1541^{+58}_{-67}	$3.053^{+0.044}_{-0.041}$
OGLE-TR-1070	$0.91^{+0.12}_{-0.15}$	$1.086^{+0.055}_{-0.060}$	$4.321^{+0.027}_{-0.027}$	5970^{+790}_{-430}	$-0.13^{+0.36}_{-3.60}$	1680^{+120}_{-100}	$0.0274^{+0.0011}_{-0.0015}$	$88.83^{+0.83}_{-1.30}$	1820^{+240}_{-130}	$1.259^{+0.063}_{-0.061}$
OGLE-TR-1071	$1.36^{+0.74}_{-0.49}$	$7.7^{+1.9}_{-1.8}$	$2.81^{+0.17}_{-0.17}$	4330^{+170}_{-170}	$0.42^{+0.13}_{-0.24}$	5500^{+1500}_{-1300}	$0.0644^{+0.0097}_{-0.0079}$	$57.8^{+7.6}_{-6.1}$	2270^{+180}_{-200}	$5.5^{+3.3}_{-2.0}$
OGLE-TR-1072	$0.97^{+0.16}_{-0.16}$	$1.140^{+0.068}_{-0.066}$	$4.311^{+0.075}_{-0.073}$	6180^{+530}_{-370}	$-0.28^{+0.37}_{-2.00}$	1491^{+96}_{-85}	$0.0271^{+0.0014}_{-0.0015}$	$84.4^{+1.8}_{-1.5}$	1930^{+180}_{-130}	$0.996^{+0.068}_{-0.065}$
OGLE-TR-1073	$1.34^{+0.54}_{-0.49}$	$3.26^{+0.82}_{-0.36}$	$3.51^{+0.16}_{-0.30}$	4550^{+170}_{-230}	$0.34^{+0.18}_{-0.29}$	2240^{+570}_{-300}	$0.0795^{+0.0093}_{-0.0110}$	$84.9^{+3.4}_{-6.3}$	1422^{+170}_{-85}	$1.110^{+0.310}_{-0.092}$
OGLE-TR-1074	$1.56^{+0.28}_{-0.25}$	$2.31^{+0.38}_{-0.24}$	$3.88^{+0.13}_{-0.12}$	6180^{+690}_{-540}	$-0.7^{+1.1}_{-2.6}$	2860^{+320}_{-290}	$0.01868^{+0.00097}_{-0.00130}$	$56.2^{+5.8}_{-7.8}$	3350^{+270}_{-220}	$1.29^{+1.10}_{-0.19}$
OGLE-TR-1075	$0.790^{+0.050}_{-0.026}$	$1.578^{+0.079}_{-0.058}$	$3.946^{+0.033}_{-0.043}$	6680^{+290}_{-250}	$-4.14^{+0.54}_{-0.12}$	2250^{+130}_{-120}	$0.1768^{+0.0036}_{-0.0020}$	$89.47^{+0.36}_{-0.42}$	962^{+41}_{-37}	$1.931^{+0.110}_{-0.073}$
OGLE-TR-1076	$0.63^{+0.13}_{-0.10}$	$1.625^{+0.093}_{-0.084}$	$3.819^{+0.044}_{-0.054}$	5380^{+180}_{-230}	$-3.45^{+0.80}_{-0.38}$	1730^{+120}_{-110}	$0.0540^{+0.0035}_{-0.0031}$	$88.73^{+0.90}_{-1.30}$	1420^{+51}_{-60}	$1.92^{+0.11}_{-0.10}$
OGLE-TR-1077	$1.36^{+0.18}_{-0.32}$	$1.67^{+0.15}_{-0.13}$	$4.116^{+0.092}_{-0.140}$	6370^{+430}_{-420}	$0.04^{+0.24}_{-0.21}$	1860^{+160}_{-140}	$0.1296^{+0.0054}_{-0.0110}$	$88.13^{+0.90}_{-0.72}$	1105^{+74}_{-57}	$1.027^{+0.078}_{-0.072}$
OGLE-TR-1078	$0.94^{+0.48}_{-0.19}$	$1.67^{+0.20}_{-0.11}$	$3.973^{+0.060}_{-0.056}$	5510^{+250}_{-220}	$-3.12^{+3.00}_{-0.64}$	1850^{+240}_{-140}	$0.0510^{+0.0075}_{-0.0037}$	$88.73^{+0.88}_{-1.50}$	1521^{+67}_{-60}	$1.397^{+0.160}_{-0.090}$
OGLE-TR-1079	$0.46^{+0.36}_{-0.15}$	$2.95^{+1.10}_{-0.60}$	$3.17^{+0.25}_{-0.30}$	4280^{+250}_{-270}	$-0.56^{+0.46}_{-0.90}$	2050^{+780}_{-400}	$0.093^{+0.017}_{-0.012}$	$85.1^{+3.4}_{-4.1}$	1170^{+150}_{-110}	$1.56^{+0.86}_{-0.43}$
OGLE-TR-1080	$1.599^{+0.130}_{-0.073}$	$2.057^{+0.120}_{-0.077}$	$4.018^{+0.025}_{-0.036}$	6230^{+320}_{-300}	$0.40^{+0.14}_{-0.22}$	2340^{+180}_{-140}	$0.06480^{+0.00170}_{-0.00098}$	$88.4^{+1.1}_{-1.5}$	1697^{+85}_{-81}	$1.334^{+0.083}_{-0.054}$
OGLE-TR-1081	$1.21^{+0.12}_{-0.15}$	$1.397^{+0.087}_{-0.081}$	$4.227^{+0.068}_{-0.075}$	5960^{+270}_{-250}	$0.25^{+0.18}_{-0.20}$	1880^{+130}_{-110}	$0.0727^{+0.0024}_{-0.0031}$	$87.38^{+0.78}_{-0.72}$	1261^{+51}_{-46}	$1.059^{+0.078}_{-0.071}$
OGLE-TR-1082	$1.034^{+0.074}_{-0.051}$	$3.15^{+0.13}_{-0.13}$	$3.459^{+0.032}_{-0.031}$	4550^{+140}_{-110}	$0.38^{+0.16}_{-0.30}$	2560^{+210}_{-160}	$0.04479^{+0.00100}_{-0.00076}$	$88.0^{+1.4}_{-2.1}$	1838^{+63}_{-53}	$1.877^{+0.081}_{-0.077}$
OGLE-TR-1083	$1.067^{+0.090}_{-0.093}$	$1.112^{+0.062}_{-0.055}$	$4.375^{+0.051}_{-0.058}$	5670^{+190}_{-180}	$0.33^{+0.14}_{-0.18}$	1468^{+87}_{-78}	$0.0624^{+0.0017}_{-0.0019}$	$87.62^{+0.70}_{-0.60}$	1155^{+44}_{-40}	$1.084^{+0.077}_{-0.068}$

continued on next page

Table 4

Continued

Name	M_* [M_\odot]	R_* [R_\odot]	logg [cgs]	T_{eff} [K]	[Fe/H] [dex]	d [pc]	a [AU]	i [deg]	T_{eq} [K]	R_p [R_J]
OGLE-TR-1084	$1.231^{+0.076}_{-0.097}$	$1.257^{+0.066}_{-0.063}$	$4.330^{+0.041}_{-0.053}$	6200^{+180}_{-180}	$0.23^{+0.18}_{-0.17}$	1320^{+57}_{-52}	$0.2445^{+0.0049}_{-0.0066}$	$89.10^{+0.11}_{-0.12}$	677^{+20}_{-19}	$1.526^{+0.100}_{-0.095}$
OGLE-TR-1085	$0.924^{+0.042}_{-0.400}$	$1.71^{+0.23}_{-0.15}$	$3.938^{+0.079}_{-0.370}$	5220^{+150}_{-350}	$-0.19^{+0.15}_{-2.50}$	1610^{+130}_{-130}	$0.04551^{+0.00091}_{-0.00730}$	$81.49^{+0.56}_{-3.70}$	1573^{+96}_{-130}	$0.942^{+0.076}_{-0.044}$
OGLE-TR-1086	$1.004^{+0.120}_{-0.090}$	$2.07^{+1.70}_{-0.47}$	$3.81^{+0.22}_{-0.51}$	5010^{+210}_{-200}	$0.00^{+0.38}_{-0.45}$	1710^{+1200}_{-350}	$0.0720^{+0.0058}_{-0.0023}$	$84.5^{+3.0}_{-6.8}$	1310^{+340}_{-140}	$1.42^{+1.90}_{-0.38}$
OGLE-TR-1087	$1.21^{+0.24}_{-0.25}$	$2.27^{+0.43}_{-0.66}$	$3.83^{+0.26}_{-0.19}$	5640^{+860}_{-730}	$0.17^{+0.26}_{-1.00}$	2400^{+410}_{-430}	$0.0565^{+0.0033}_{-0.0041}$	$82.6^{+4.8}_{-2.8}$	1660^{+190}_{-120}	$1.79^{+0.44}_{-0.59}$
OGLE-TR-1088	$0.860^{+0.064}_{-0.084}$	$0.972^{+0.030}_{-0.035}$	$4.398^{+0.019}_{-0.022}$	5670^{+620}_{-230}	$-0.17^{+0.17}_{-1.60}$	954^{+33}_{-31}	$0.0553^{+0.0014}_{-0.0017}$	$89.40^{+0.42}_{-0.58}$	1145^{+120}_{-46}	$1.187^{+0.040}_{-0.037}$
OGLE-TR-1089	$1.259^{+0.089}_{-0.100}$	$1.294^{+0.087}_{-0.086}$	$4.317^{+0.049}_{-0.059}$	6050^{+240}_{-240}	$0.434^{+0.092}_{-0.160}$	1480^{+110}_{-110}	$0.2910^{+0.0067}_{-0.0080}$	$89.42^{+0.21}_{-0.16}$	614^{+29}_{-27}	$1.72^{+0.13}_{-0.14}$
OGLE-TR-1090	$1.38^{+0.16}_{-0.26}$	$1.83^{+0.25}_{-0.11}$	$4.044^{+0.072}_{-0.150}$	6490^{+340}_{-320}	$-0.12^{+0.16}_{-0.47}$	2130^{+180}_{-140}	$0.0771^{+0.0031}_{-0.0048}$	$87.7^{+1.5}_{-2.0}$	1548^{+85}_{-66}	$1.283^{+0.230}_{-0.091}$
OGLE-TR-1091	$0.146^{+0.100}_{-0.036}$	$0.971^{+0.082}_{-0.069}$	$3.63^{+0.22}_{-0.13}$	3670^{+170}_{-100}	$-1.40^{+0.67}_{-1.00}$	620^{+65}_{-53}	$0.164^{+0.026}_{-0.016}$	$88.92^{+0.37}_{-0.29}$	431^{+34}_{-32}	$1.073^{+0.100}_{-0.088}$
OGLE-TR-1092	$1.16^{+0.14}_{-0.16}$	$2.59^{+0.17}_{-0.30}$	$3.707^{+0.086}_{-0.140}$	4804^{+250}_{-83}	$0.20^{+0.20}_{-0.26}$	2292^{+500}_{-15}	$0.0493^{+0.0024}_{-0.0028}$	$78.8^{+2.3}_{-1.0}$	1690^{+78}_{-51}	$1.043^{+0.170}_{-0.046}$
OGLE-TR-1093	$1.59^{+0.26}_{-0.18}$	$3.61^{+0.32}_{-0.29}$	$3.518^{+0.110}_{-0.079}$	5220^{+590}_{-290}	$0.17^{+0.27}_{-0.45}$	2710^{+480}_{-260}	$0.0317^{+0.0014}_{-0.0011}$	$57.4^{+3.4}_{-3.5}$	2700^{+220}_{-120}	$3.82^{+0.92}_{-1.10}$
OGLE-TR-1094	$1.005^{+0.042}_{-0.053}$	$1.65^{+0.17}_{-0.22}$	$4.005^{+0.120}_{-0.087}$	4990^{+170}_{-160}	$0.35^{+0.14}_{-0.35}$	1450^{+130}_{-140}	$0.1095^{+0.0015}_{-0.0019}$	$89.19^{+0.58}_{-0.88}$	930^{+43}_{-45}	$1.62^{+0.16}_{-0.21}$
OGLE-TR-1095	$1.83^{+4.40}_{-0.89}$	$2.04^{+0.21}_{-0.18}$	$4.11^{+0.46}_{-0.29}$	9500^{+17000}_{-3100}	$-1.8^{+1.6}_{-1.7}$	5500^{+5900}_{-2100}	$0.0205^{+0.0100}_{-0.0040}$	$69.9^{+14.0}_{-9.9}$	4600^{+6000}_{-1200}	$1.062^{+0.110}_{-0.092}$
OGLE-TR-1096	$0.968^{+0.060}_{-0.110}$	$3.51^{+0.12}_{-0.15}$	$3.328^{+0.023}_{-0.023}$	4560^{+220}_{-120}	$0.05^{+0.34}_{-0.62}$	2880^{+230}_{-150}	$0.04410^{+0.00090}_{-0.00170}$	$88.4^{+1.1}_{-1.7}$	1967^{+95}_{-56}	$2.446^{+0.080}_{-0.089}$
OGLE-TR-1097	$0.873^{+0.140}_{-0.089}$	$0.874^{+0.074}_{-0.072}$	$4.514^{+0.056}_{-0.064}$	6200^{+1200}_{-1400}	$-1.0^{+1.3}_{-2.5}$	1280^{+840}_{-580}	$0.0926^{+0.0046}_{-0.0032}$	$88.08^{+0.22}_{-0.24}$	920^{+190}_{-220}	$1.017^{+0.096}_{-0.093}$
OGLE-TR-1098	$1.09^{+0.15}_{-0.16}$	$1.272^{+0.079}_{-0.082}$	$4.262^{+0.066}_{-0.072}$	5960^{+470}_{-290}	$0.16^{+0.25}_{-0.54}$	2070^{+160}_{-150}	$0.0656^{+0.0029}_{-0.0035}$	$86.06^{+0.46}_{-0.45}$	1264^{+110}_{-64}	$1.76^{+0.13}_{-0.14}$
OGLE-TR-1099	$1.01^{+0.81}_{-0.40}$	$8.1^{+2.2}_{-1.8}$	$2.63^{+0.23}_{-0.20}$	4460^{+180}_{-200}	$-0.26^{+0.18}_{-0.47}$	5500^{+1700}_{-1300}	$0.107^{+0.017}_{-0.015}$	$70.9^{+3.8}_{-4.1}$	1870^{+170}_{-150}	$4.2^{+2.0}_{-1.1}$

REFERENCES

- Alard, C., and Lupton, R.H. 1998, *ApJ*, **503**, 325.
- Bakos, G. and Noyes, R.W. and Kovács, G., *et al.* 2004, *PASP*, **116**, 266.
- Baluev, R. 2012, *MNRAS*, **422**, 2372.
- Bouchy, F., Pont, F., Santos, N., *et al.* 2004, *A&A*, **421**, L13.
- Borucki, W. Koch, D., Basri, G., *et al.* 2010, *Science*, **327**, 977.
- Chambers, K., Magnier, E., Metcalfe, N., *et al.* , 2016, [arXiv:1612.05560](#), .
- Charbonneau, D., Brown, T., Latham, D., and Mayor, M. 2000, *ApJ*, **529**, L45.
- Choi, J., Dotter, A., Conroy, C., *et al.* *ApJ*, **2016**, **823**, 102.
- Cumming, A., Butler, R., Marcy, G., *et al.* 2008, *PASP*, **120**, 531.
- Eastman, J., Siverd, R., and Gaudi, S. 2010, *PASP*, **122**, 935.
- Eastman, J., Rodriguez, J., Agol, E., *et al.* , 2019, [arXiv:1907.09480](#), .
- Gaia Collaboration, Montegriffo, P., Bellazzini, M., *et al.* 2023a, *A&A*, **674**, A33.
- Gaia Collaboration, Vallenari, A., Brown, A., *et al.* 2023b, *A&A*, **674**, A1.
- Gonzalez, O., Rejkuba, M., Zoccali, M., *et al.* 2012, *A&A*, **543**, A13.
- Gould, A., Huber, D., Penny, M., and Stello, D. 2015, *Journal of Korean Astronomical Society*, **48**, 93.
- Guo, X., Johnson, J., Mann, A., *et al.* 2017, *ApJ*, **838**, 25.
- Hagey, S.R., Edwards, B., and Boley, A.C. 2022, *AJ*, **164**, 220.
- Henry, G., Marcy, G., Butler, R., and Vogt, S. 2000, *ApJ*, **529**, L41.
- Hippke, M. and Heller, R. 2019, *A&A*, **623**, A39.
- Howard, A., Marcy, G., Bryson, S., *et al.* 2012, *ApJS*, **201**, 15.
- Konacki, M., Torres, G., Jha, S., and Sasselov, D. 2003a, *Nature*, **421**, 507.
- Konacki, M., Torres, G., Sasselov, D., and Jha, S., 2003b, *ApJ*, **597**, 1076.
- Kovács, G. and Zucker, S. and Mazeh, T. 2002, *A&A*, **391**, 369.
- Mandel, K. and Agol, E. 2002, *ApJ*, **580**, L171.
- Mayor, M., Marmier, M., Lovis, C., *et al.* 2011, , [arXiv:1109.2497](#), .
- Mazeh, T., Holczer, T., and Faigler, S. 2016, *A&A*, **589**, A75.
- Melo, C., Santos, N., Pont, F., *et al.* 2006, *A&A*, **460**, 251.
- Montet, B., Yee, J. and Penny, M. 2017, *PASP*, **129**, 044401.
- Morton, T. 2012, *ApJ*, **761**, 6.
- Morton, T. 2016, *ApJ*, **822**, 86.
- Nataf, D., Gould, A., Fouqué, P., *et al.* 2013, *ApJ*, **769**, 88.
- Penny, M., Gaudi, B., and Kerins E. *et al.* 2019, *ApJS*, **241**, 3.
- Pollacco, D., Skillen, I., and Collier Cameron, A. 2006, *PASP*, **118**, 1407.
- Pont, F., Bouchy, F., and Queloz, D., *et al.* 2004, *A&A*, **426**, L15.
- Pont, F., Zucker, S., Queloz, D. 2006, *MNRAS*, **373**, 231.
- Pont, F., Tamuz, O., Udalski, A., *et al.* 2008, *A&A*, **487**, 749.
- Ricker, G., Winn, J., Vanderspek, R., *et al.* 2015, *Journal of Astronomical Telescopes, Instruments, and Systems*, **1**, 014003.
- Saydjari, A., Schlafly, E., Lang, D., *et al.* 2023, *ApJ*, **264**, L28.
- Sahu, K., Casertano, S., Bond, H., *et al.* 2006, *Nature*, **443**, 534.
- Sahu, K., Casertano, S., Valenti, J., *et al.* 2008, *ASPC*, **398**, 93.
- Soszyński I., Pawlak M., Pietrukowicz P., *et al.* 2016, *Acta Astron.*, **66**, 405.
- Spergel, D., Gehrels, N., Baltay, C., *et al.* 2015, , [arXiv:1503.03757](#), .
- Udalski, A., Paczyński K., Źebruń, K., *et al.* 2002a, *Acta Astron.*, **52**, 1.
- Udalski, A., Źebruń, K., Szymański, M., *et al.* 2002b, *Acta Astron.*, **52**, 115.
- Udalski, A., Szewczyk, O., Źebruń, *et al.* 2002c, *Acta Astron.*, **52**, 317.
- Udalski, A., Pietrzyński, G., Szymański, M., *et al.* 2003, *Acta Astron.*, **53**, 133.
- Udalski, A., Szymański, M., Kubiak, M., *et al.* 2004, *Acta Astron.*, **54**, 313.
- Udalski, A., Pont, F., Naef, C., *et al.* 2008, *A&A*, **482**, 749.

- Udalski, A., Szymański, M., and M. Szymański, G. 2015, *Acta Astron.*, **65**, 1.
West, R., Pollacco, D., Wheatley, P., *et al.* 2016, *The Messenger*, **165**, 10.
Woźniak, P.R. 2000, *Acta Astron.*, **50**, 421.
Zhu, W., and Dong, S. 2021, *ARA&A*, **59**, 291.